Rocketdyne R-6777

INVESTIGATION OF VARIABLES IN TURBINE EROSION, DROPLET FORMATION AND MATERIAL DAMAGE WITH STEAM

By

R. Spies

November 1966

prepared for

NATIONAL AERONAUTICS AND SPACE ADMINISTRATION

Contract NAS7-391

ROCKETDYNE
A Division of North American Aviation, Inc.,
6633 Canoga Avenue, Canoga Park, California

ROCKETDYNE • A DIVISION OF NORTH AMERICAN AVIATION, INC.

Rocketdyne R-6777

INVESTIGATION OF VARIABLES IN TURBINE EROSION, DROPLET FORMATION AND MATERIAL DAMAGE WITH STEAM

By

R. Spies

November 1966

prepared for

NATIONAL AERONAUTICS AND SPACE ADMINISTRATION

Contract NAS7-391

ROCKETDYNE
A Division of North American Aviation, Inc.,
6633 Canoga Avenue, Canoga Park, California

FOREWORD

This report was prepared by Rocketdyne, a Division of North American Aviation, Inc. in compliance with G. O. 8738 under NASA Contract NAS7-391. The work was administered under the technical direction of the Jet Propulsion Laboratory with Mr. Lance Hays acting as Technical Manager. The report summarizes the work performed during the period 30 June 1965 to 31 October 1966. The Rocketdyne designation for this report is R-6777. Participation of Messrs. J. R. Baughman, P. C. Thys, U. J. Vandenberg, D. H. Cooke, and R. M. Rattray of Rocketdyne in this program is acknowledged.

ABSTRACT

A program to investigate the effect of variables on turbine erosion is now in progress. Tests have been made with steam to determine the size, velocity, and origin of drops propagating through a typical stage of a space power turbine. Test conditions were chosen to simulate the passage of potassium vapor through the same turbine stage so that correlation with potassium-vapor experiments would be possible in the future. High-speed photographs have been obtained of the vapor flow to evaluate the erosion hazard to turbine blades.

To evaluate material characteristics, turbine blades made of four different materials were run in the same wheel. Comparative weight-loss data and rate-of-loss data permit evaluation based on material properties. This evaluation is continuing. Tests with different quality, speed, and nozzle-to-rotor spacing are being conducted. Future reports will be issued on the results of these investigations.

CONTENTS

ILLUSTRATIONS

TABLES

INTRODUCTION

Erosion of turbine blades has been encountered in Rankine-cycle powerplants for many years. In central stations, this problem has usually been solved by the application of special materials and by systematic replacement of blades. While this procedure may be costly, it has been effective. The literature is full of articles which deal with the prevention of erosion, elimination of the damaging water, special blade shapes, alteration of spacing, etc. Yet, no solution has been found which is universally acceptable. In fact, it becomes increasingly clear as the literature is surveyed that the process of erosion is but little understood.

In space power systems of large power output (300 kilowatts to multimegawatt), the Rankine cycle is of considerable interest. The working fluid for such a cycle may well be an alkali metal, with potassium as the prevalent choice. Such a system is surely prone to erosion if conditions are right. Two major differences from the stationary steam powerplant are evident. First, space-system requirements usually include a need for 10,000 hours plus of unattended operation. This precludes replacement as a solution to blade erosion. Second, space systems employ turbines which are small, high-speed machines; diameters of less than 1 foot, blade heights of 1 inch, and rotative speeds of 30,000 rpm are common. It is not immediately evident whether small, lightly loaded blades erode in a manner similar to large, highly loaded ones.

To determine what some of the significant variables in the erosion of potential space power turbines might be, a program was undertaken under NASA sponsorship at Rocketdyne.* Basic testing including direct observation of the droplet formation, and impact was to be done. It was evident

*Contract NAS7-391 administered through the Jet Propulsion Laboratory

that the basic two-phase flow and impact phenomena are not well understood and that the number of variables is too great for a completely analytical determination of their effects upon erosion.

DROPLET FORMATION

While complete understanding of the causes of turbine blade erosion is not available, certain conclusions can be drawn. As the vapor expands through the turbine, the saturation line is reached. While some amount of supersaturation is possible, a point is finally reached where condensation begins. The size of the droplets formed during this condensation depends on many things (e.g., vapor temperature, pressure, and rate of expansion) but they are generally agreed to be in the submicron diameter range (1 micron = 10^{-6} meters). The drops are therefore of small mass and they are rapidly accelerated to nearly free-stream velocity. For this reason, these drops encounter the moving turbine blades at nearly the correct vector velocity and have little (if any) impact with the blades. As these drops pass through successive stages, they grow and may impinge on subsequent nozzle walls. Here they merge with drops which may be condensing on the wall and form attached drops of sizable magnitude. Eventually they reach a size where the drop is stripped from the wall and re-enters the moving stream. Such drops have diameters in the range of 50 to 1000 microns depending on the conditions of the flow; therefore they have large mass and they are accelerated slowly. Upon leaving the nozzle, their absolute velocity is much lower than the free-stream velocity, and their velocity relative to the blade is large and in the wrong direction. Figure 1 demonstrates a typical condition. Amelioration of erosion can be expected by:

1. Decreasing the number of large drops by changing turbine geometry

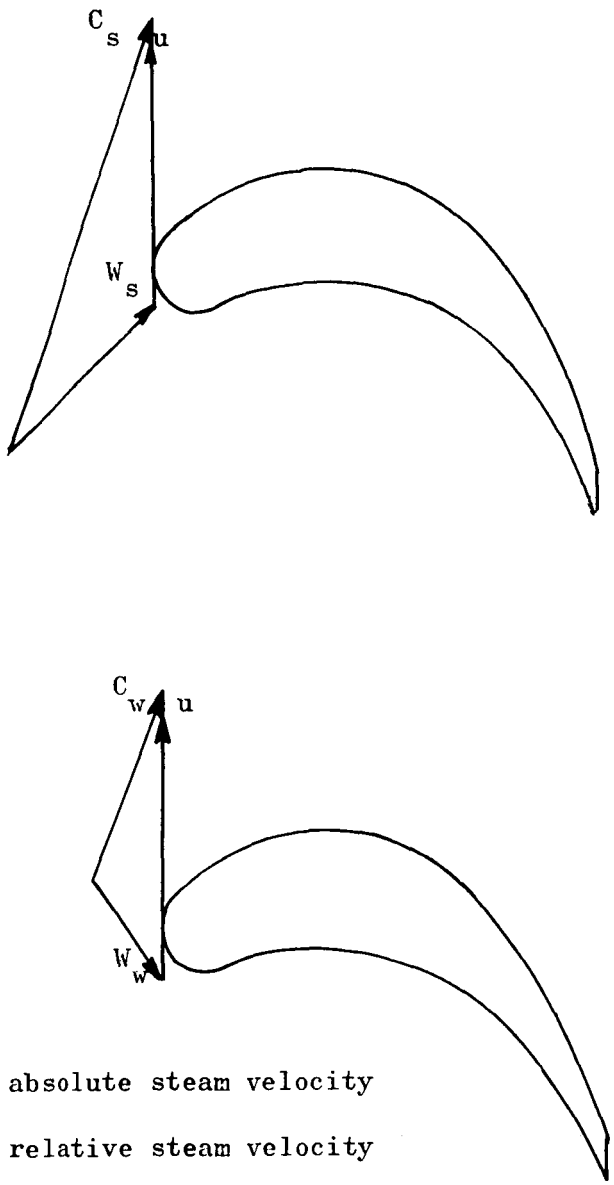

C_s = absolute steam velocity

W_s = relative steam velocity

C_w = absolute water velocity

W_w = relative water velocity

u = blade velocity

Figure 1. Velocity Diagram for Turbine Blade

2. Increasing nozzle-blade spacing to provide more time for droplet acceleration and breakup

3. Draining of droplets before they leave the stator

MATERIAL CONSIDERATIONS

Erosion can be prevented or reduced to a tolerable level by increasing the resistance of the blade material to the liquid impact. In central power stations, stellite facing has been used at the leading edges of the rotor blades. However, problems of speed, temperature, and material compatibility encountered in space power machinery make this solution insufficient. It is evident, therefore, that a more complete understanding of the erosion mechanism and the metallographic effects is desirable.

The exact nature of the metallographic interaction with the impacting drop is the subject of a number of research projects at this time. In general, correlation of erosion resistance with any one material property has not been successful. However, evidence exists that some form of fatigue mechanism is responsible for erosion, and that some form of the endurance fatigue limit may make correlation possible. Material hardness is also under consideration as a correlation parameter. To a large degree, hardness is reflected in the fatigue endurance limit used in the determination of the material threshold velocity. For ferrous and some aluminum alloys, hardness is a direct measure of the material's tensile strength, and for most materials, fatigue strength increases with tensile strength. As part of the program described here, turbine blades of four different materials were fabricated to determine what differences in erosion resistance occurred when the blades were exposed to the identical liquid impact conditions.

TEST FLUID

Although the ultimate fluid of interest for a space power system is an an alkali metal, probably potassium, the initial test program to evaluate erosion was performed using steam. The reasons for this choice were: (1) large body of literature with which to correlate, (2) ease of testing and inspection of parts, (3) ability to visualize flow so that the conditions of liquid impact are known for steam and can be estimated for later potassium tests, and (4) elimination of corrosion as a variable.

Great care was exercised to choose test conditions which would be dynamically similar to conditions in a potassium system. Considerations used were: (1) similar droplet sizes, (2) similar velocity vectors, and (3) similar material properties. A detailed account of the similarity conditions is given below.

OBJECTIVE OF THE PROGRAM

The objective of the program is to investigate the effects of vapor quality, droplet size and velocity, and turbine geometry on turbine erosion with wet vapor. To do this, a special test turbine was run to correlate local measurement of droplet size, velocity, and trajectory with observed erosion patterns on different blade geometries and materials. Particular emphasis was placed on mechanical erosion with chemical effects minimized or isolated as much as possible.

These tests were run using steam. Experiments were structured so that future tests using a liquid metal will be directly comparable. This is done by testing with hardware identical to hardware to be used for liquid-metal testing in the potassium turbine loop available at Rocketdyne, and at conditions which provide similar droplet size, impact location, and impact stress.

PROGRAM TASKS

The program was divided into six tasks:

TASK I	Turbine Test Rig Fabrication
TASK II	Measurement Apparatus
TASK III	Fabrication of Turbine Wheel and Housing
TASK IV	Testing
TASK V	Evaluation of Results
TASK VI	Laser Pulsing System

Progress in each of these areas is discussed.

TURBINE TEST RIG FABRICATION

TEST RIG

A two-stage test turbine (Fig. 2) was designed and fabricated for the steam test series. The turbine wheels used in this design were fabricated from Waspalloy in anticipation of a possible requirement for future potassium testing. The shaft is supported on two water-lubricated journal bearings and one double-acting water-lubricated thrust bearing. Provision is made for a plastic window covering the second stage, making it possible to observe droplet formation and propagation through that stage. Basic dimensions of the unit are shown in Table 1. Figure 3 shows the assembled rotor.

Because it was necessary to test more than one blade material at the same time to obtain a comparative assessment, provision was made in the second turbine stage for demountable blades. The blades were cast, and a fir-tree section conforming to a Rocketdyne standard was ground into the root. The wheel was broached to accept these blades. Figure 4 shows the turbine wheels.

TEST LOOP

A special steam test loop was assembled by Rocketdyne for use on these tests. Figure 5 is an overall view of the facility with key components identified. A loop line diagram is shown in Fig. 6. Specifications include

Boiler:

flow	1700 lb/hr
pressure	150 to 500 psi
quality	99.6 percent

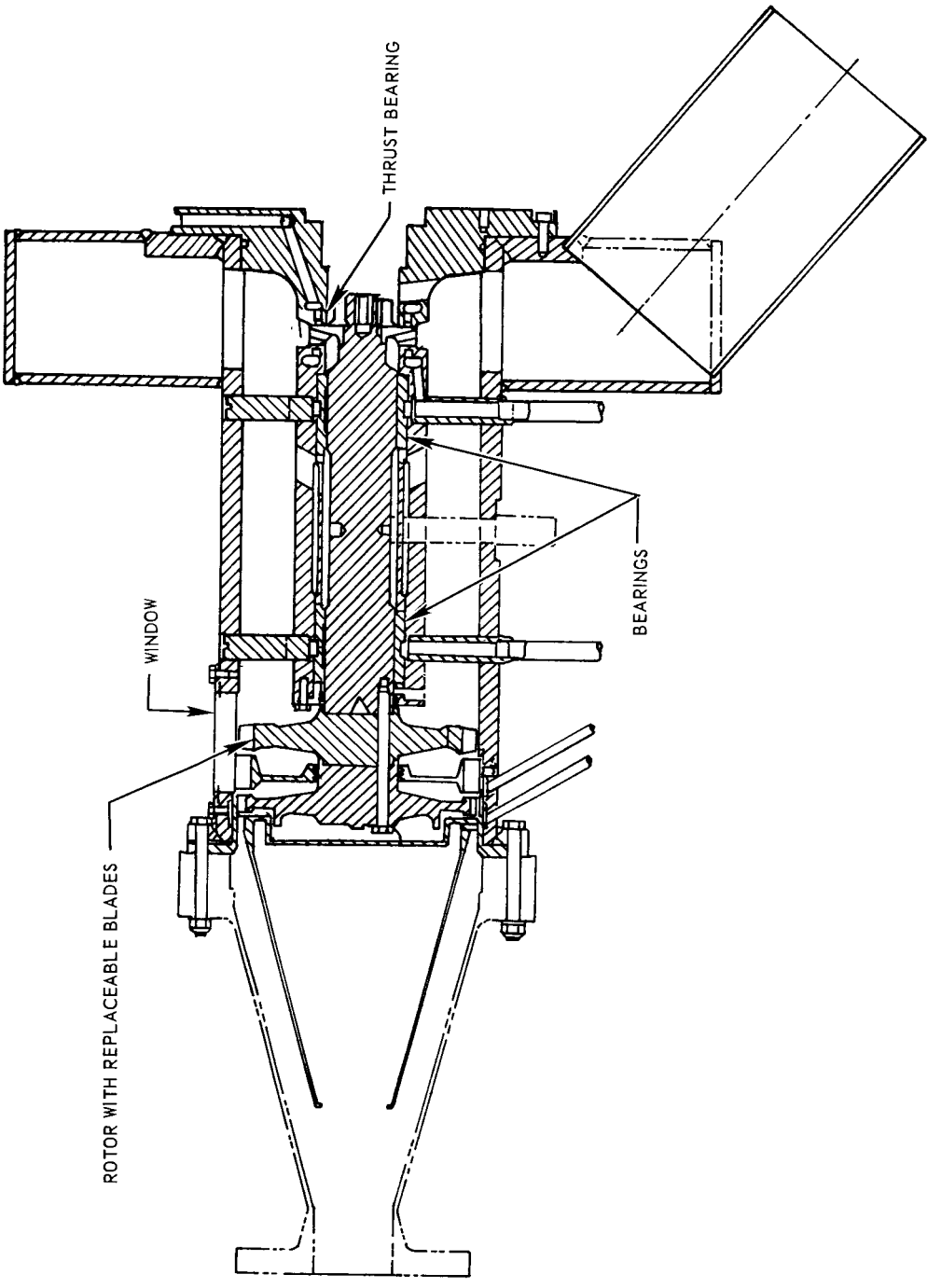

Figure 2. Erosion Test Turbine Assembly

TABLE 1

EROSION TEST TURBINE DESIGN

Number of Stages	2
Tip Diameter	
First Stage, inches	6.00
Second Stage, inches	6.16
Design Speed, rpm	29,700
Design Tip Velocity	
First Stage, ft/sec	777
Second Stage, ft/sec	800
Design Flow, lb/hr	500
Design Inlet Pressure, psia	13.75
Design Inlet Moisture, percent	6.4
Design Outlet Pressure, psia	2.25
Design Outlet Moisture, percent	11

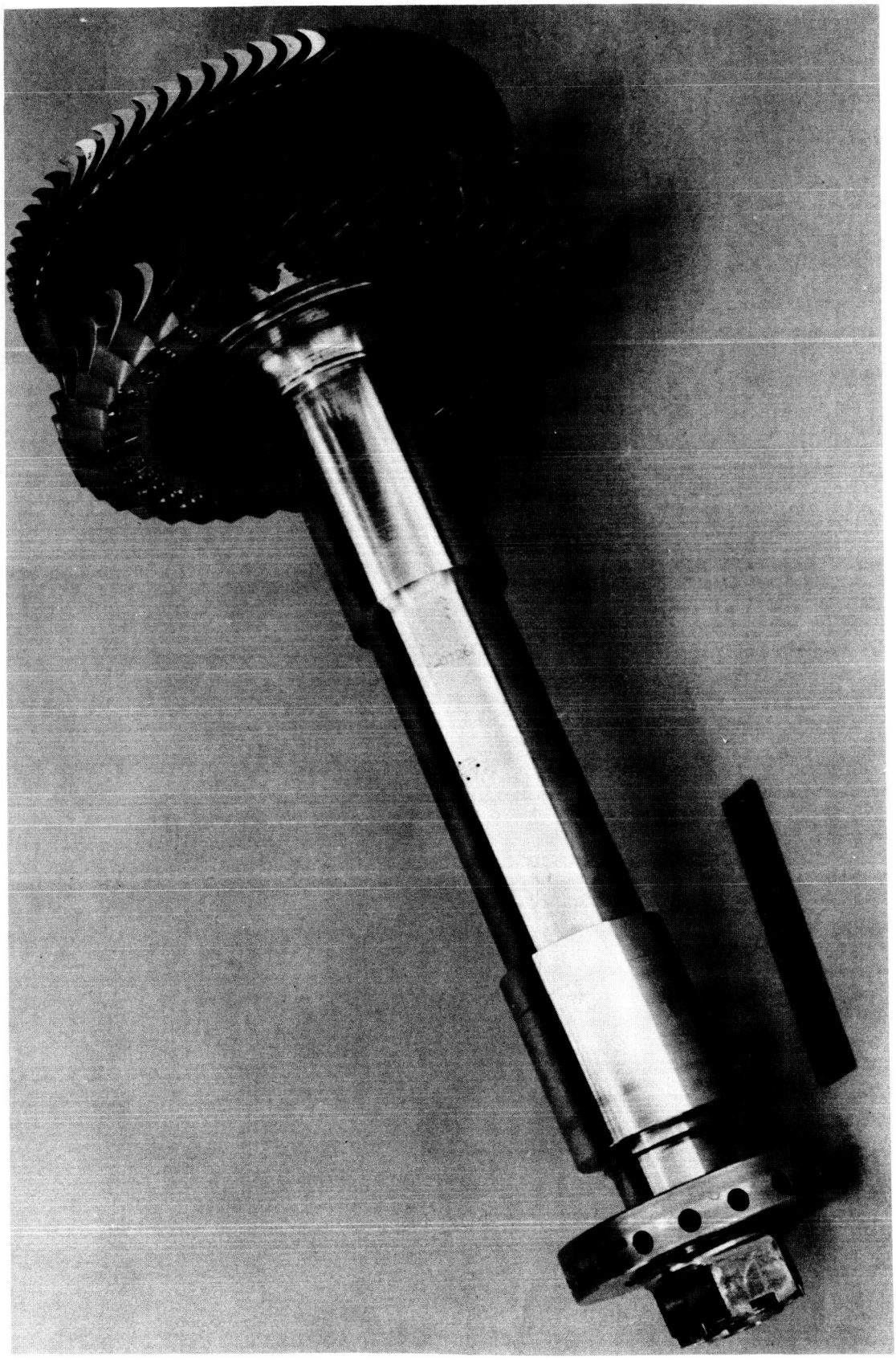

1XY55-9/21/66-C1B

Figure 3. Turbine Rotor

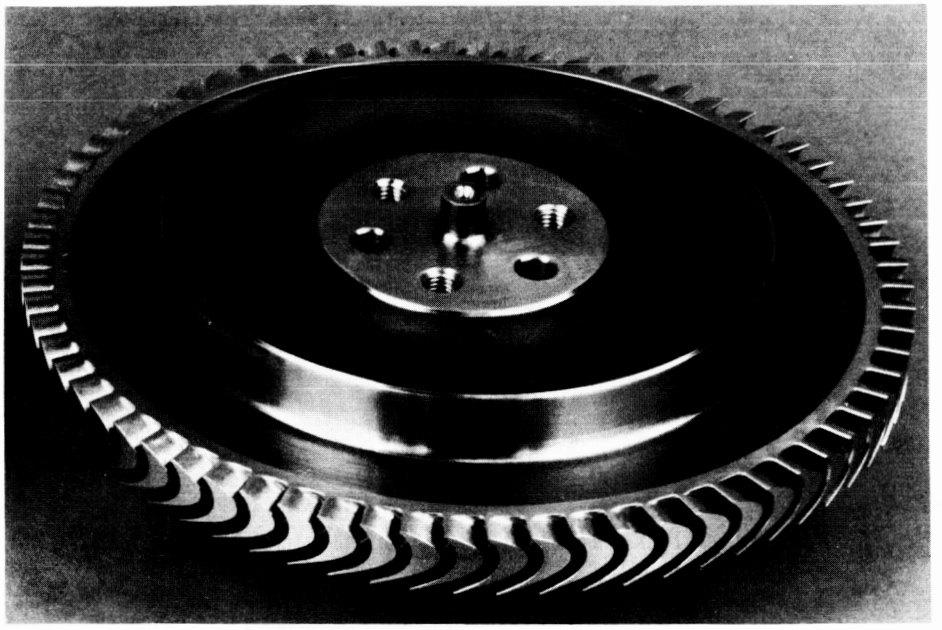

First Stage

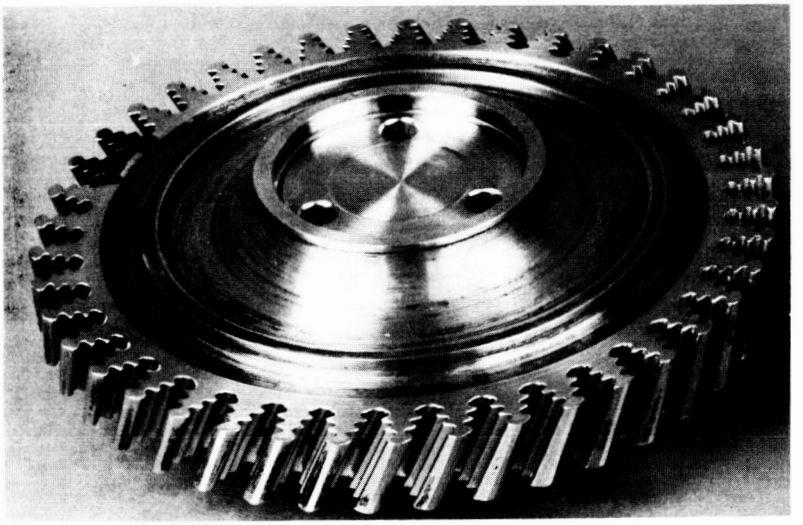

Second Stage

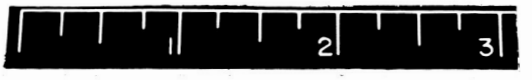

Figure 4. Erosion-Turbine Wheels

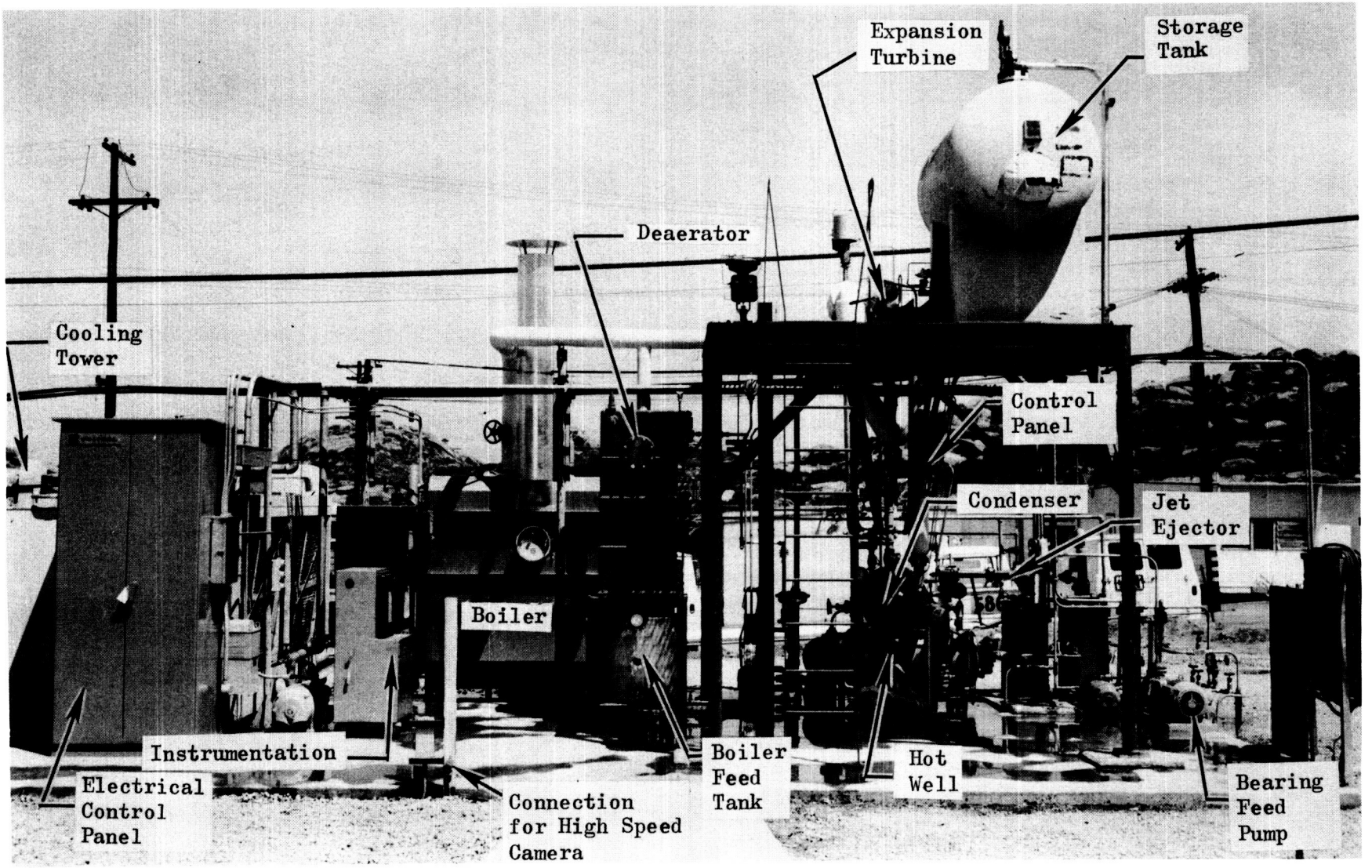

3XA55-7/22/66-S

Figure 5. Steam Test Facility

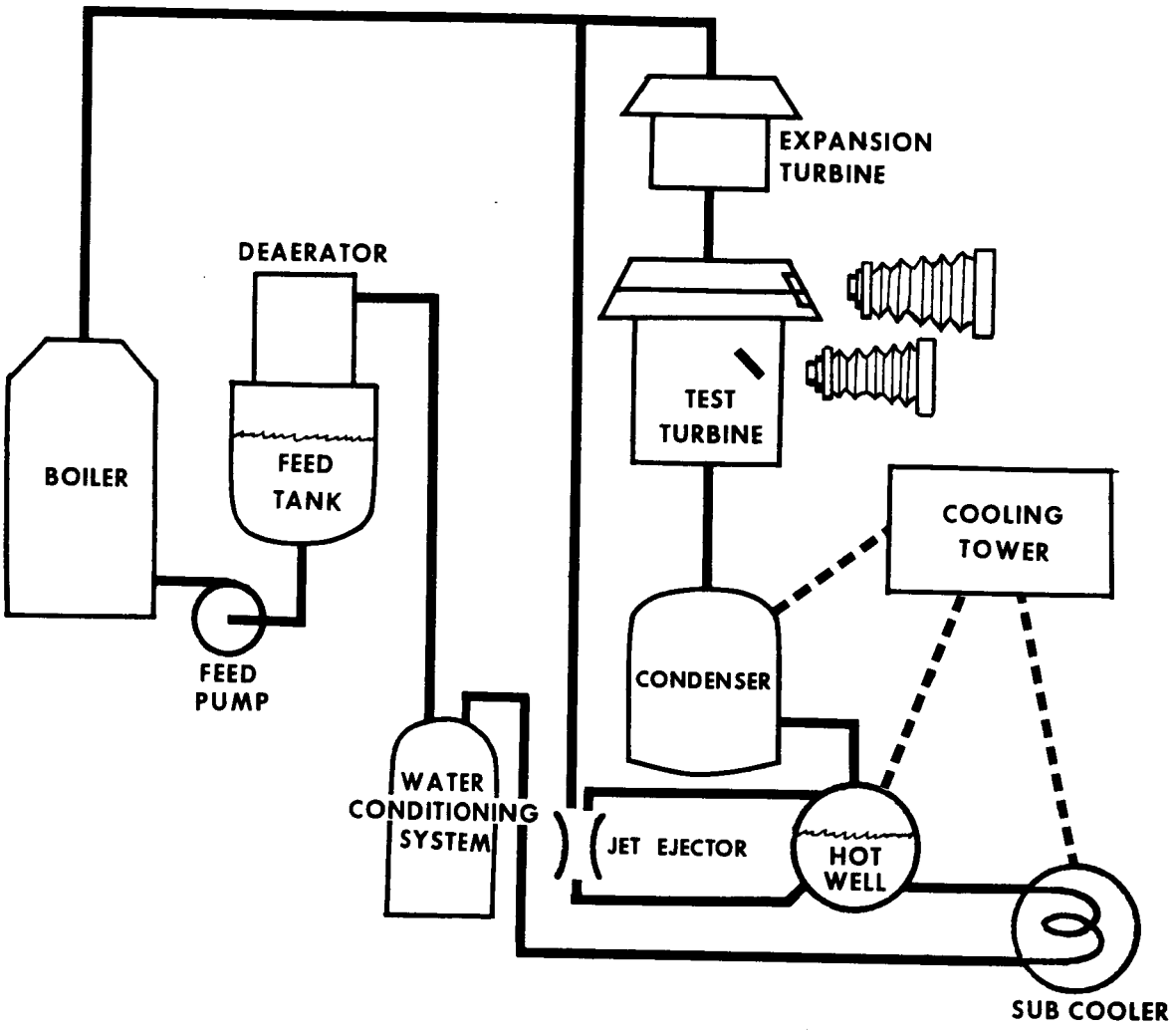

Figure 6. Steam Test Facility Schematic

Condenser:	
heat rate	1.6×10^6 Btu/hr
pressure	2 to 5 psia
Deaerator:	
content	less than 0.005 cc/liter
Jet Ejector:	
pressure	1 inch Hg absolute

SIMILARITY PARAMETERS *

One of the requirements for the steam tests was that similarity to conditions anticipated in a potassium turbine stage would be maintained. In this way, future tests using potassium would yield data directly relatable to the results obtained. Geometric similarity was ensured by using turbine components identical to those which would be used in a potassium test (stator and rotor).

To ensure dynamic similarity, the drop sizes to be expected as a result of condensation, agglomeration, and shedding must be determined. The exact nature of these processes is not understood, although much work is in process at this time. It is generally agreed that the nucleation process is rate dependent (Ref. 1); that steam will exhibit supersaturation; that the submicron-sized condensation products will not play a major role in blade erosion. The droplets resulting from agglomeration on nozzle walls are the drops of major concern to this study. Their size may depend on a number of physical conditions related to the velocity distribution, such as the nature of the boundary layer, the wakes behind the trailing edge, the trailing edge thickness, and the secondary flow field. These conditions are dealt with in detail in Ref. 2.

*In this section, design considerations are reviewed. A discussion of the formulation of the various parameters is given in Appendix A.

A review of the literature done early in this program revealed three types of drop-size correlation. In Ref. 3, Gardner stipulates that the size of a droplet torn from a puddle by a moving gas or vapor stream is the same as that of a droplet suddenly thrown into the stream. For this condition

$$\frac{\rho U^2 d_c}{\sigma} = 13$$

where

ρ = vapor density

U = vapor velocity

d_c = critical droplet size

σ = liquid surface tension

This dimensionless number is the ratio of the drag forces to the surface tension forces and is referred to as the Weber Number (We). For equal vapor velocity and droplet size, the correlating parameter between two flow conditions becomes

$$\frac{\sigma}{\rho} = \text{constant}$$

Figure 7 shows the variation of σ/ρ for steam and potassium as a function of temperature.*

In rocket engine technology, the combustion of propellant depends to a large degree on the type of droplets formed. Investigation along these lines at Rocketdyne evolved a correlation based on

$$Re^m We^n = \text{constant}$$

*Values for surface tension used are shown in Appendix B.

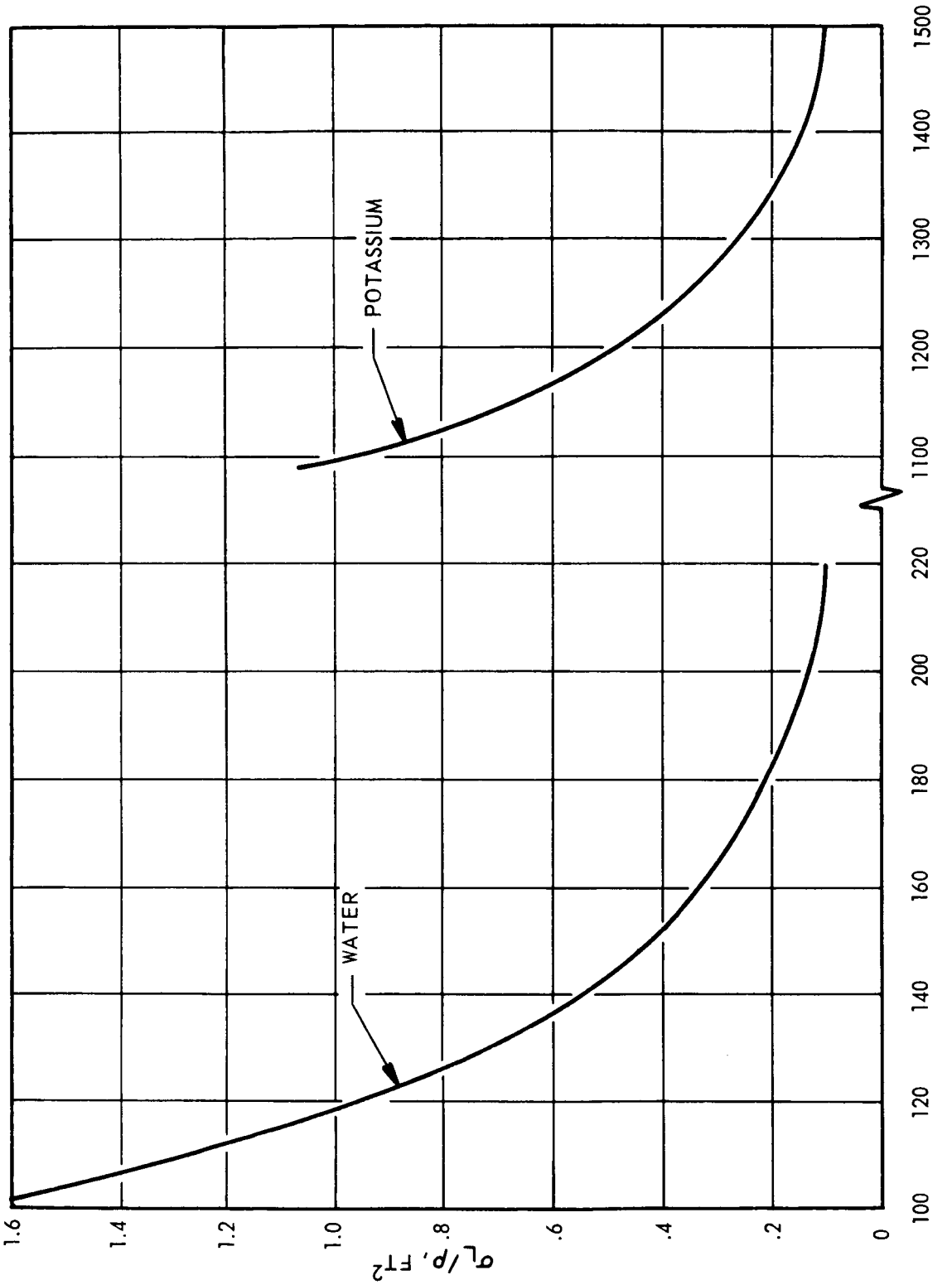

Figure 7. Surface Tension to Vapor Density Ratio vs Temperature for Water and Potassium (Significant Parameter Where We = Constant for Critical Droplet Diameter)

where

$$Re = \text{Droplet Reynolds Number} = \frac{\rho U d_c}{\mu}$$

and

μ = viscosity of the vapor

The Reynolds Number is the ratio of inertia and viscous forces. Two types of relations were found in Ref. 4 ,

$$ReWe = \text{constant}$$

and

$$\frac{We}{Re^{1/2}} = \text{constant}$$

The latter was subsequently confirmed by data in Ref. 5 . Bennett-Cowell in a discussion to Ref. 3 quotes the ReWe = constant relationship and attributes it to Hanson, et al. (Ref. 6).

The formulation ReWe = constant can be written as

$$\frac{\rho^2 U^3 d_c^2}{\sigma \mu} = \text{constant}$$

and for equal velocity and drop size, the correlating parameter between two flow conditions becomes

$$\frac{\sqrt{\sigma \mu}}{\rho} = \text{constant}$$

For $We/Re^{1/2}$,

$$\frac{\rho U^3 d_c \mu}{\sigma^2} = \text{constant}$$

and the parameter is

$$\frac{\sigma^2}{\rho \mu} = \text{constant}$$

Figures 8 and 9 show these two conditions.

A fourth correlation could be based on Reynolds Number alone. In this case

$$\frac{\rho U d_c}{\mu} = \frac{U d_c}{\nu} = \text{constant}$$

where

$$\nu = \frac{\mu}{\rho} = \text{kinematic viscosity}$$

and correlation involves only the kinematic viscosity as shown in Fig. 10.

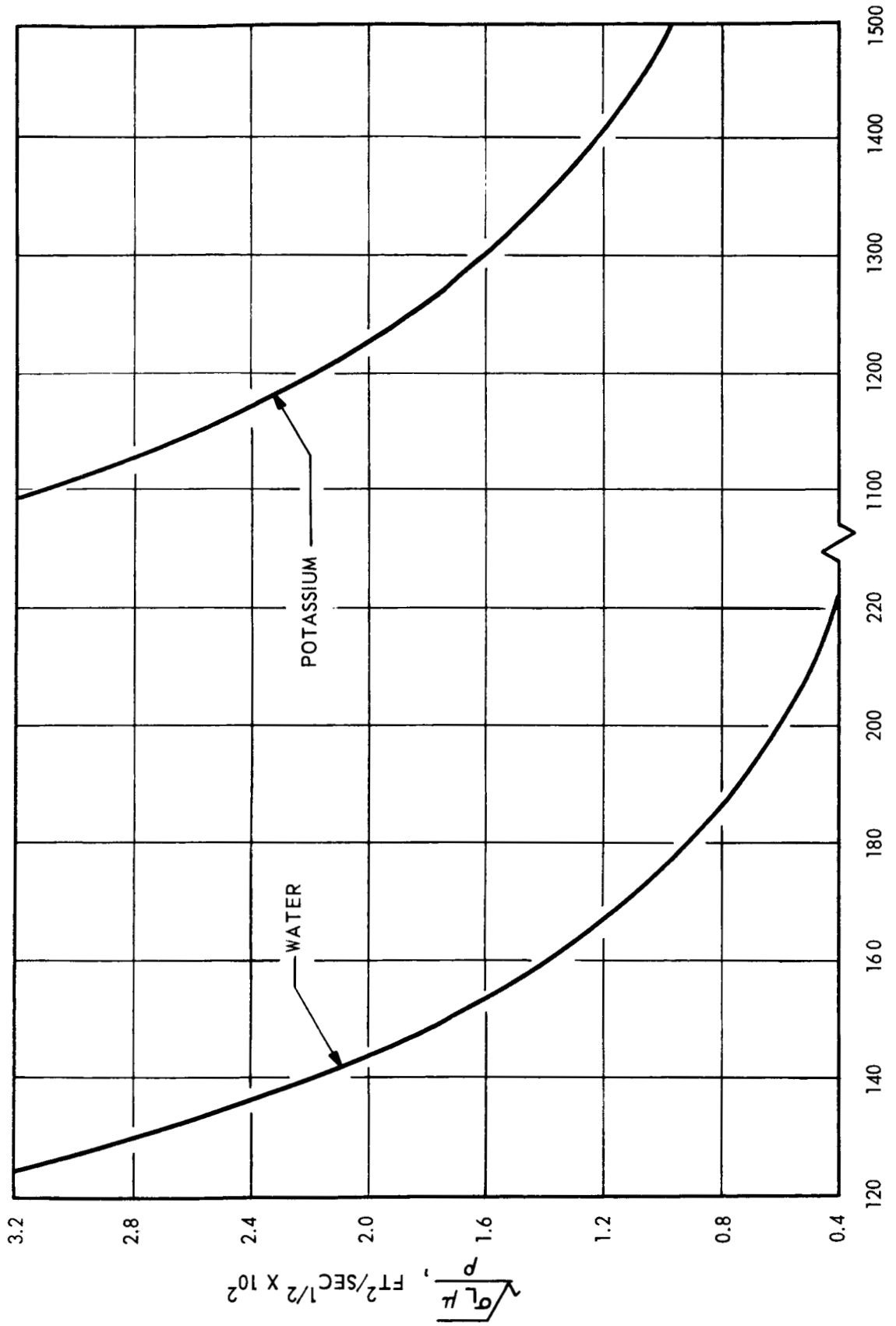

Figure 8. Ratio of Square Root of Product of Surface Tension and Vapor Viscosity to Vapor Density for Water and Potassium (Significant Parameter Where Weke = Constant for Critical Droplet Diameter)

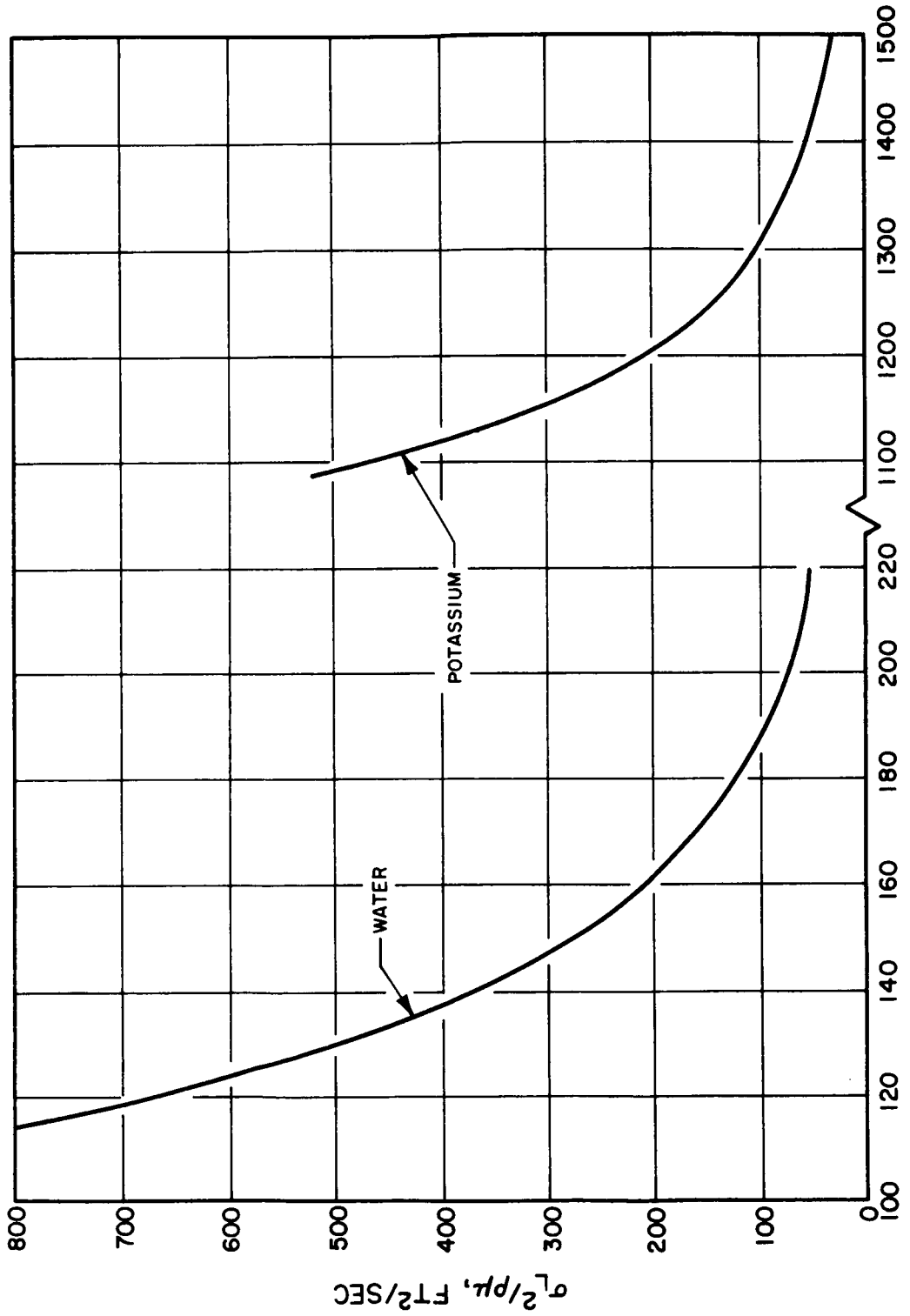

Figure 9. Ratio of Surface Tension Squared to Product of Vapor Density and Viscosity for Water and Potassium (Significant Parameter Where $We/Re^{1/2}$ = Constant for Critical Droplet Diameter)

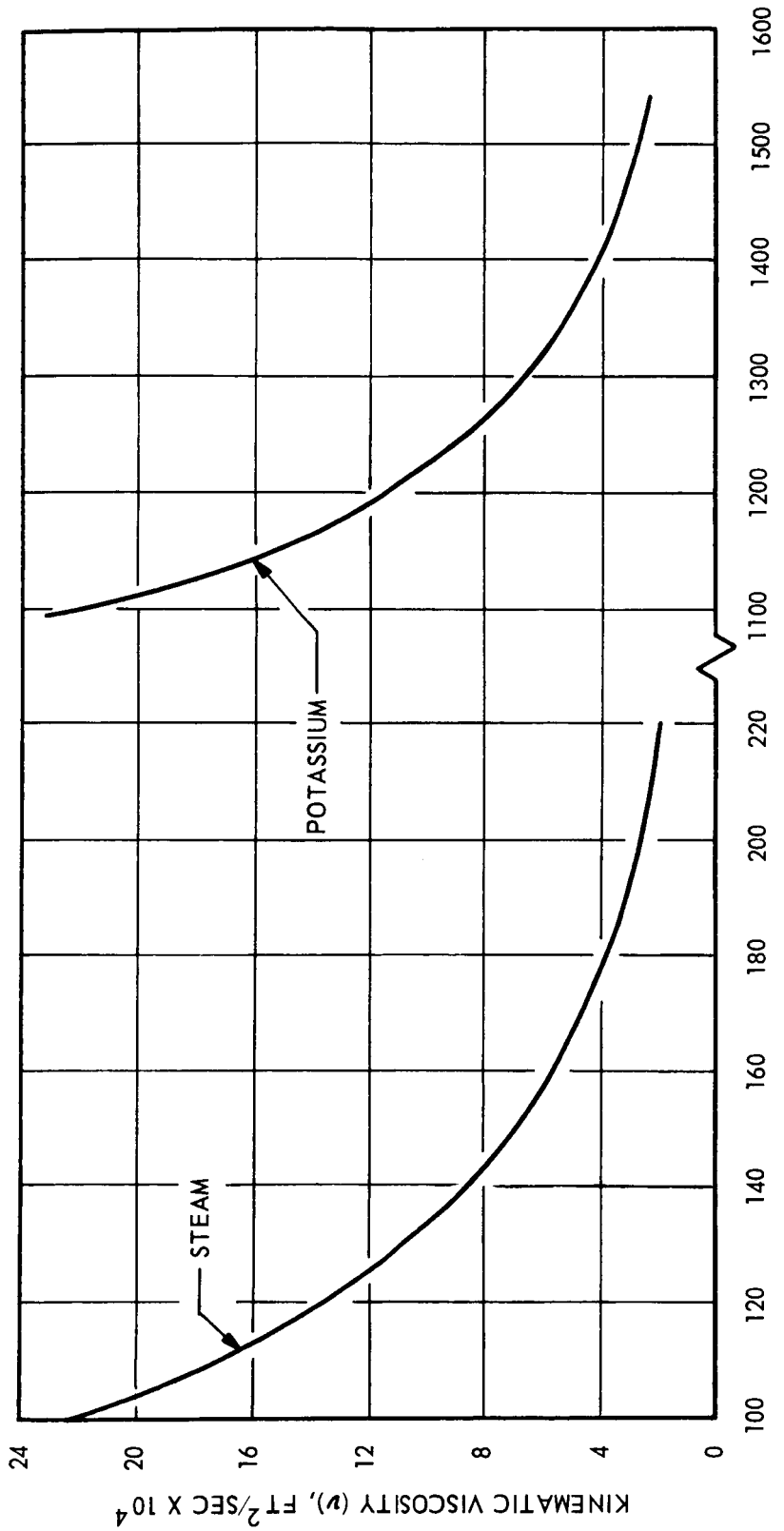

Figure 10. Kinematic Viscosity of Steam and Potassium Vapor vs Temperature (Significant Parameter for Re = Constant)

At this time it is not evident which, if any, of these correlations are applicable to the tests being conducted. It is, however, of great interest to study the conditions in potassium which would correspond to a given condition of steam. For purposes of comparison, the conditions in potassium vapor corresponding to steam at 130 F are listed in Table 2.

TABLE 2

CORRELATION OF POTASSIUM TO 130 F STEAM

Criterion	Significant Parameter	Drop Size (Micron) at 1000 ft/sec	
		Steam at 130F	Potassium at 1160F
We = 13	σ_L/ρ = constant	92	82
$We/Re^{1/2} = 1$	$\sigma_L^2/\rho\,\mu$ = constant	188	108
WeRe = 4000	$\sqrt{\sigma_L\,\mu}/\rho$ = constant	95	85
Re = 380	ν = constant	125	167

It is obvious that, regardless of which criterion is chosen for the design of the test parameters, potassium at approximately 1160 F will produce droplets which are of the same size as those produced in 130 F steam. Furthermore, because the Reynolds number will be nearly the same, the flow field (wake, secondary flow) will be similar. The turbine test rig and test loop were, therefore, designed for the 130 F steam condition to simulate the potassium flow in a late stage of a potassium turbine.

MEASUREMENT APPARATUS

The objective of this program includes the measurement of the droplets impacting on the moving blades (diameter and speed) and the observation of their behavior. The size of the droplets to be observed has a distinct bearing on the measurement apparatus. In the previous section, a determination of the probable size was shown to be the function of certain flow criteria; the choice of criterion was left undetermined. For purposes of design, the droplet size occurring in each case can be determined, as shown in Table 3.

TABLE 3

CRITICAL DROPLET DIAMETERS,
STEAM AT 130 F

Condition	Diameter, microns	
	U=300	U=1000
We = 13	1020	92
$\frac{We}{Re^{1/2}} = 1$	5700	188
WeRe = 4000	578	95
Re = 380	417	125

The droplets which must be measured are, therefore, of considerable size, and are amenable to photographic recording and measurement. It is, of course necessary to take pictures at a framing rate and exposure time which will stop the droplet motion.

Within the nozzle and at its exit, droplet motion will be slow, on the order of 100 to 300 ft/sec. At a framing rate of 6000 frames per second, a droplet will translate from 0.2 to 0.6 inch between frames. Recording with a Fastax camera is, therefore, sufficient to record this phenomenon. Subsequent projection on a Vanguard analyzer yields magnification for measurement of the droplet diameter and motion. In the gap between the nozzle and moving blade row, velocities in excess of 1000 ft/sec will be observed. Much greater camera framing rates and smaller exposure times will, therefore, be required. The use of a high-speed Beckman and Whitley camera is planned. As will be described in the section on Laser Pulsing Systems, use of a laser is contemplated as a high-speed light source.

NOZZLE TESTS

To determine the possibility of measuring the size and velocity of the droplets which propagate through, and agglomerate in the turbine nozzle, a series of tests were made to photograph the drops. As a secondary objective for these tests, the comparative effects of creating wet steam by expansion through a turbine and by injection of water were evaluated.

Preliminary Nozzle Test Loop

While the nozzle test loop was being assembled, preliminary checks were made using a small, existing steam loop. This test setup is shown in Fig. 11. The boiler, located out of sight on the left, delivers steam through the injection venturi to the test chamber. The recording camera, a Fastax camera using a high magnification lens, and the power supply for a pulsed Xenon light source which is synchronized with the camera are also shown.

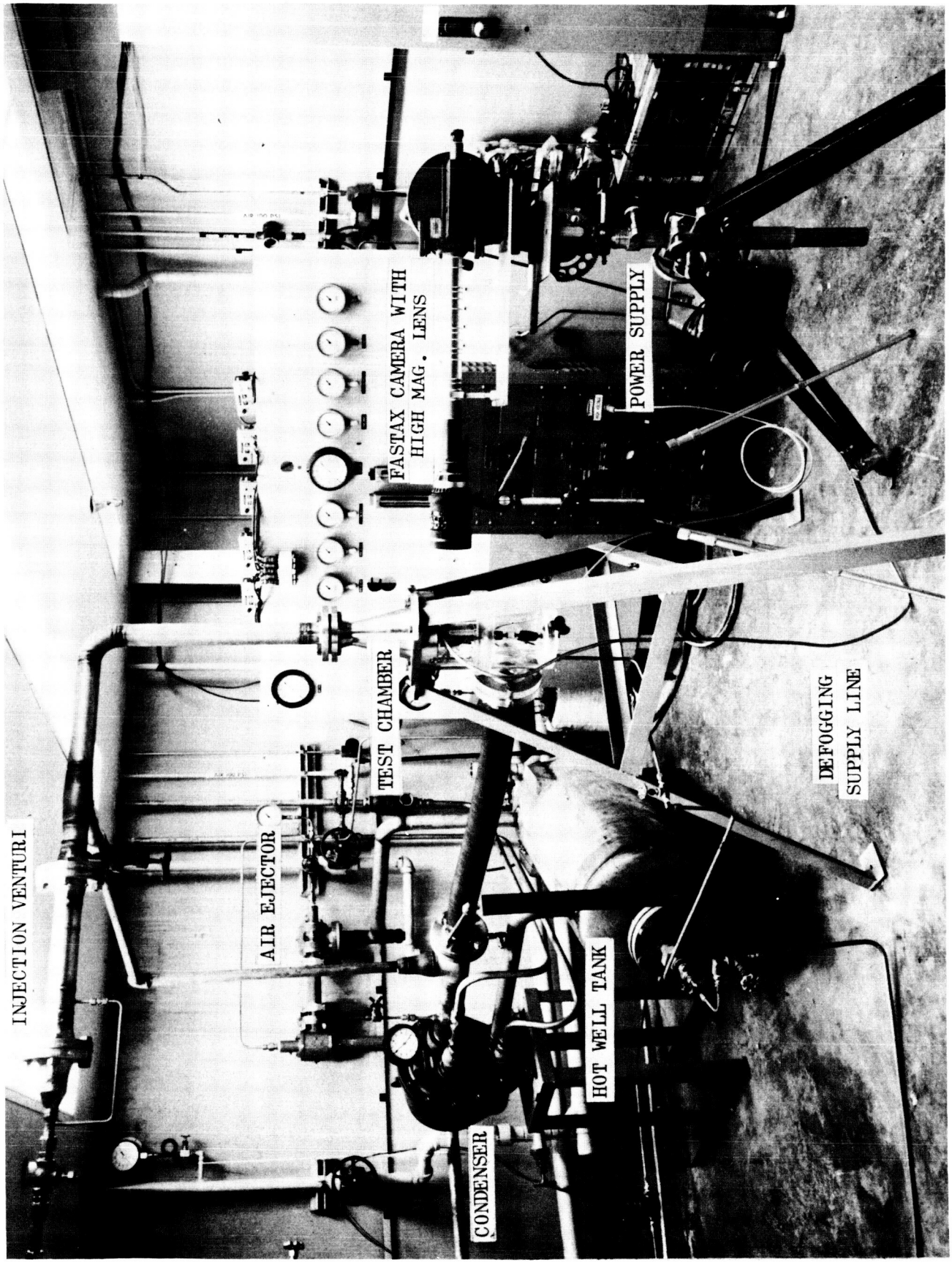

Figure 11. Preliminary Nozzle Test Loop

The test rig used for these initial tests was identical with that used in the later nozzle tests. It consists of a nozzle diaphragm mounted in a flanged inlet cone, with a cast acrylic exhaust chamber through which the high-speed photographs are taken. The nozzle diaphragm is essentially the same as the design for the high moisture stage of the rotating tests. The exhaust chamber consists of two concentric tubes with the resulting annulus closed at one end and open to the nozzle flow at the other. To avoid thermal expansion problems, the entire exhaust chamber is fabricated from acrylic, including a tangential flanged exit pipe which is connected to the loop exhaust piping through a flexible joint. The open end of the chamber is pressed against the nozzle face through gaskets by relatively long bolts to permit radial expansion relative to the nozzle face. The region inside the inner acrylic tube is open to the atmosphere to permit placement of the light source system. A closed box-shaped hole has been provided in both tubes to permit placement of a mirror for an axial view of the nozzle trailing edges.

The nozzle block can be seen in the mirror in Fig. 12. Figure 13 shows the general shape and dimensions of the nozzles tested. The tests were run at nozzle exit pressures of 2.5 to 3 psia and vapor velocities of 600 and 1200 ft/sec. The nozzle inlet moisture content was approximately 8 percent for all runs as obtained by injection of a metered amount of distilled water into the vapor stream at the throat of a special venturi between the boiler and the nozzle block. Observation of the high-speed films obtained in these tests showed the occurence of accumulated puddles of water which remained attached to the trailing edge at about the center of the wake as shown in Fig. 14. These puddles were subject to constant rippling and distortion under the buffeting of the wake turbulence. At random intervals, droplets and sheets were stripped off and entrained in the vapor stream, frequently in considerable profusion. British researchers have reported similar phenomena except that pendulous drops

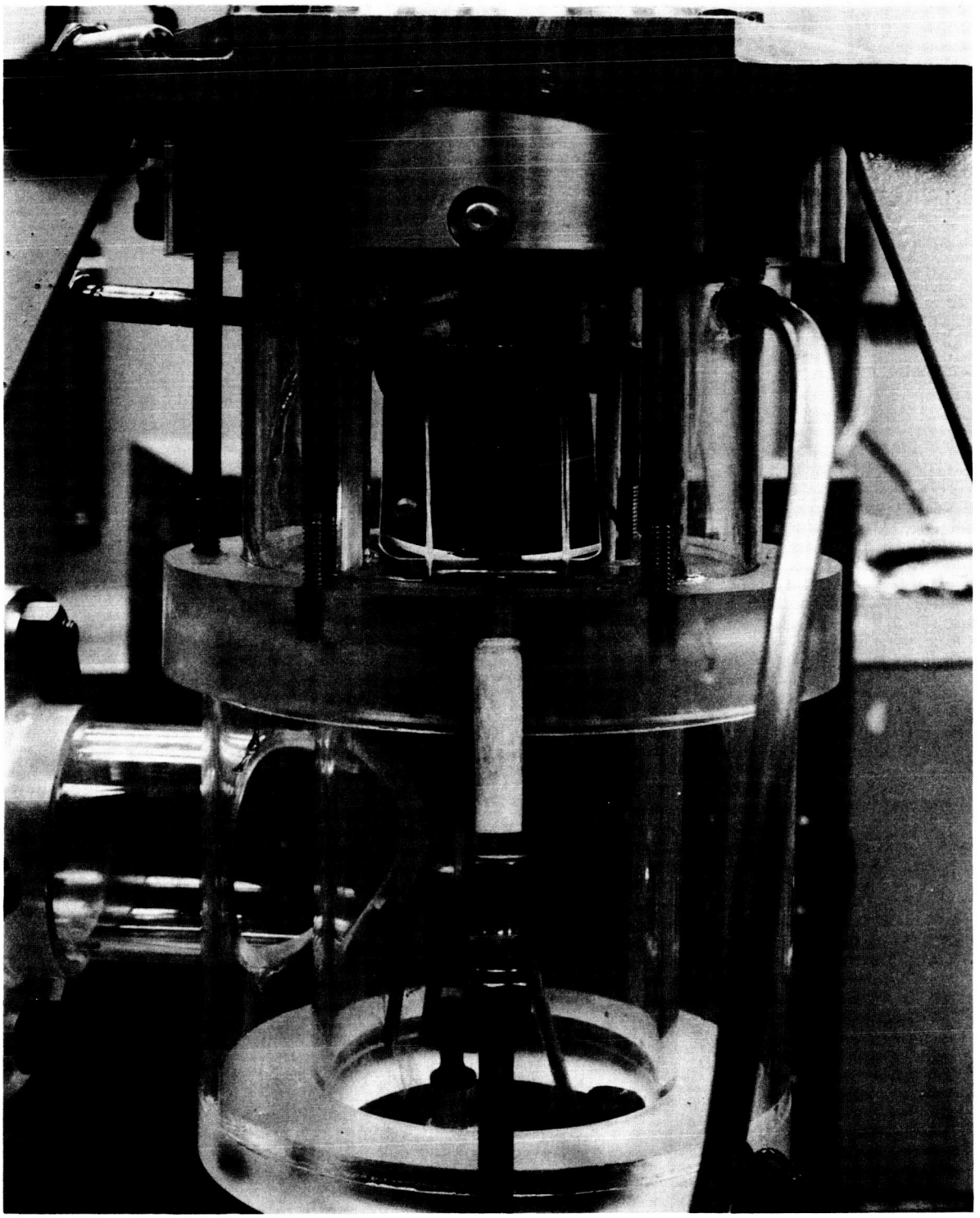

5AJ35-12/6/65-C1B

Figure 12. Nozzle Test Rig Assembly

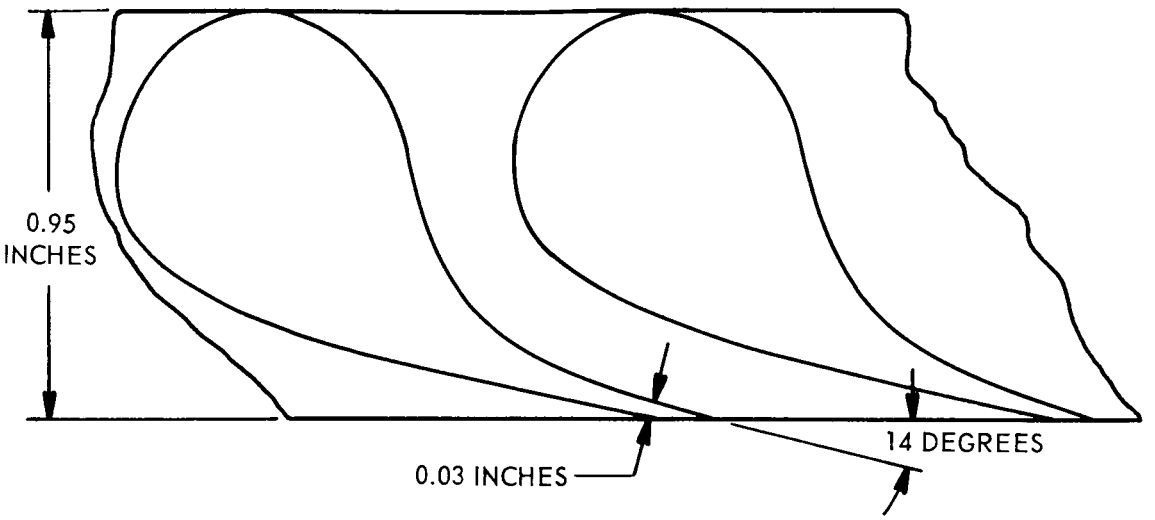

SECTION A-A

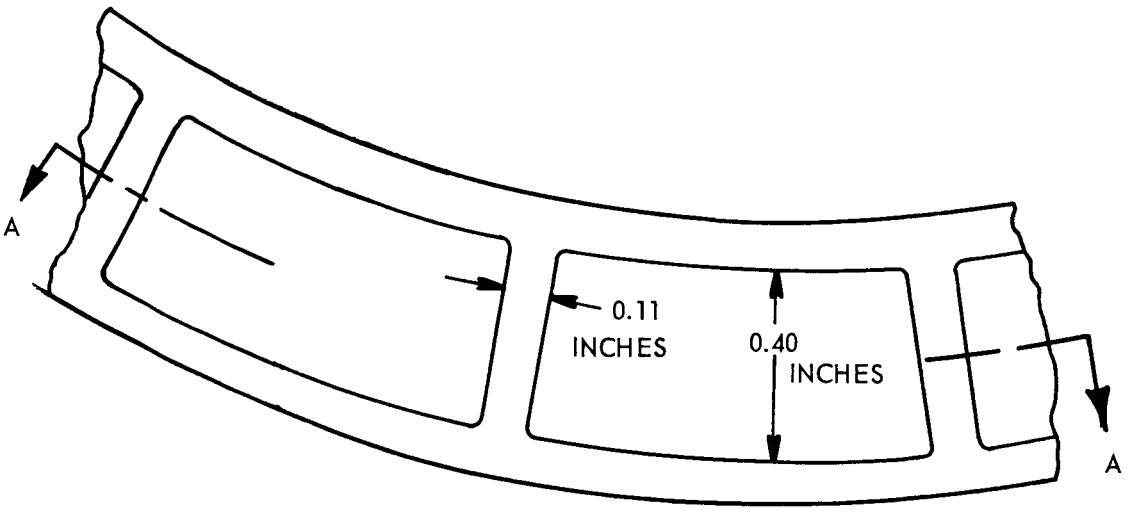

RADIAL VIEW

Figure 13. Nozzle Dimensions

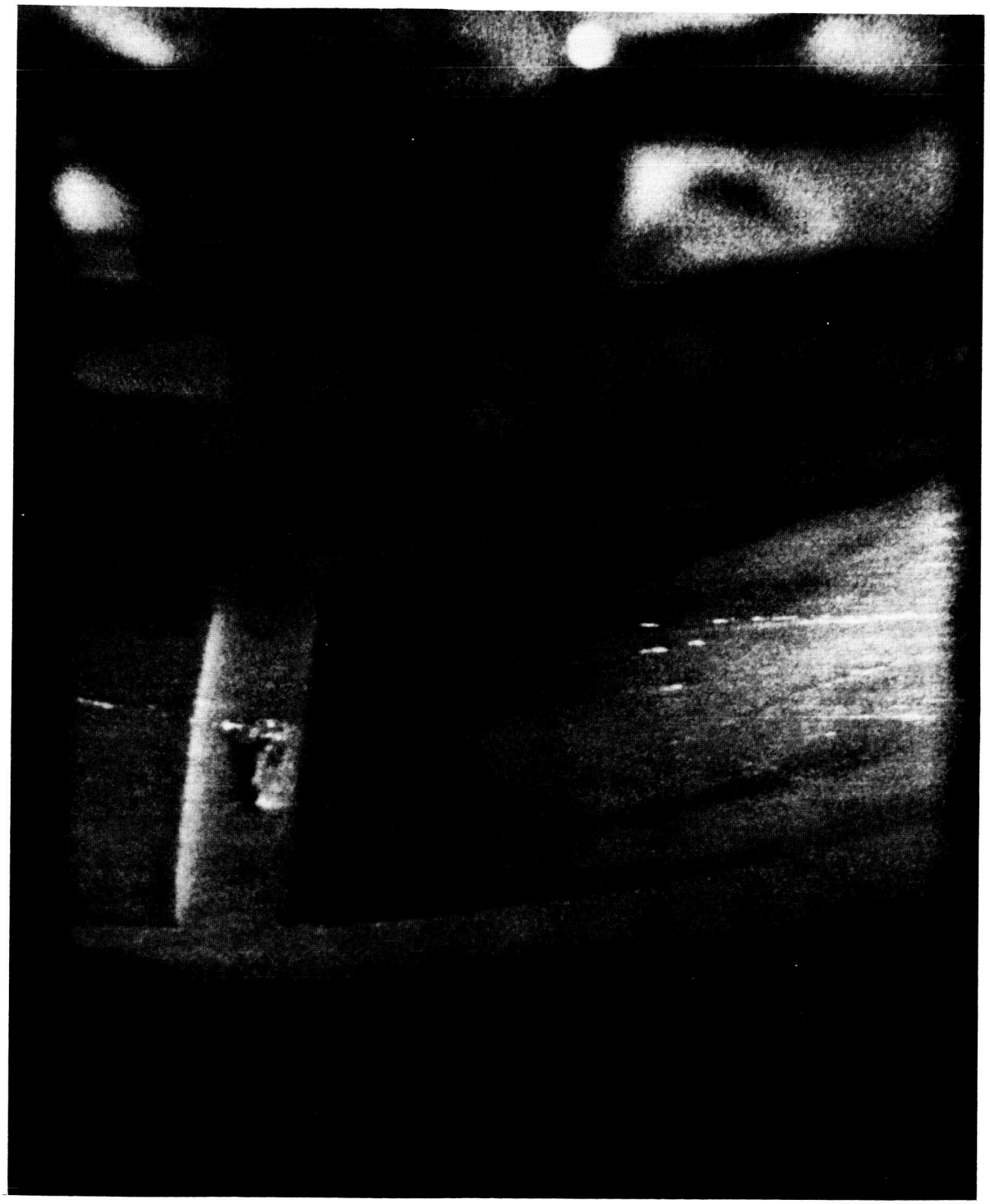

Figure 14. Streams on Suction Surface

rather than flat puddles were observed by them. This is probably due to the shape of the trailing edge of the stator blade. It was also noted that the motion of the puddles was quite irregular compared to the periodic motion of the pendulous drops as reported by Hays (Ref. 7).

For the lower vapor velocity runs (600 ft/sec), a single puddle was formed near the center of the blade span as in Fig. 14. For the 1200 ft/sec runs, several puddles were formed. It is significant that the puddles formed near the center of the span rather than near the tip as in observations with long narrow nozzles such as used in large, low pressure turbines.

The shedding of droplets from the trailing edge was not confined to stripping from the puddles. Narrow streams running the visible length of the suction surface fed the puddles, but some also ran off the edge without apparent buildup or hesitant action. The streams may be seen on two adjacent suction surfaces in Fig. 14. The rippling of the flow in the relatively fixed streams may be observed in sequences of many frames. The sweep of the streams toward the tip (on the suction surface) by the secondary flow vortices is also seen in the films.

An interesting observation about the feeding of the puddles was that they apparently were fed from the pressure surface as well as from the suction surface. Review of some films shows the onset of the puddle with the liquid coming from the acute edge and gradually moved toward the larger puddles nearer the center.

A closeup of drops being stripped from one of the puddles is shown in Fig. 15. The stripping starts as a long tongue with a rather thin neck

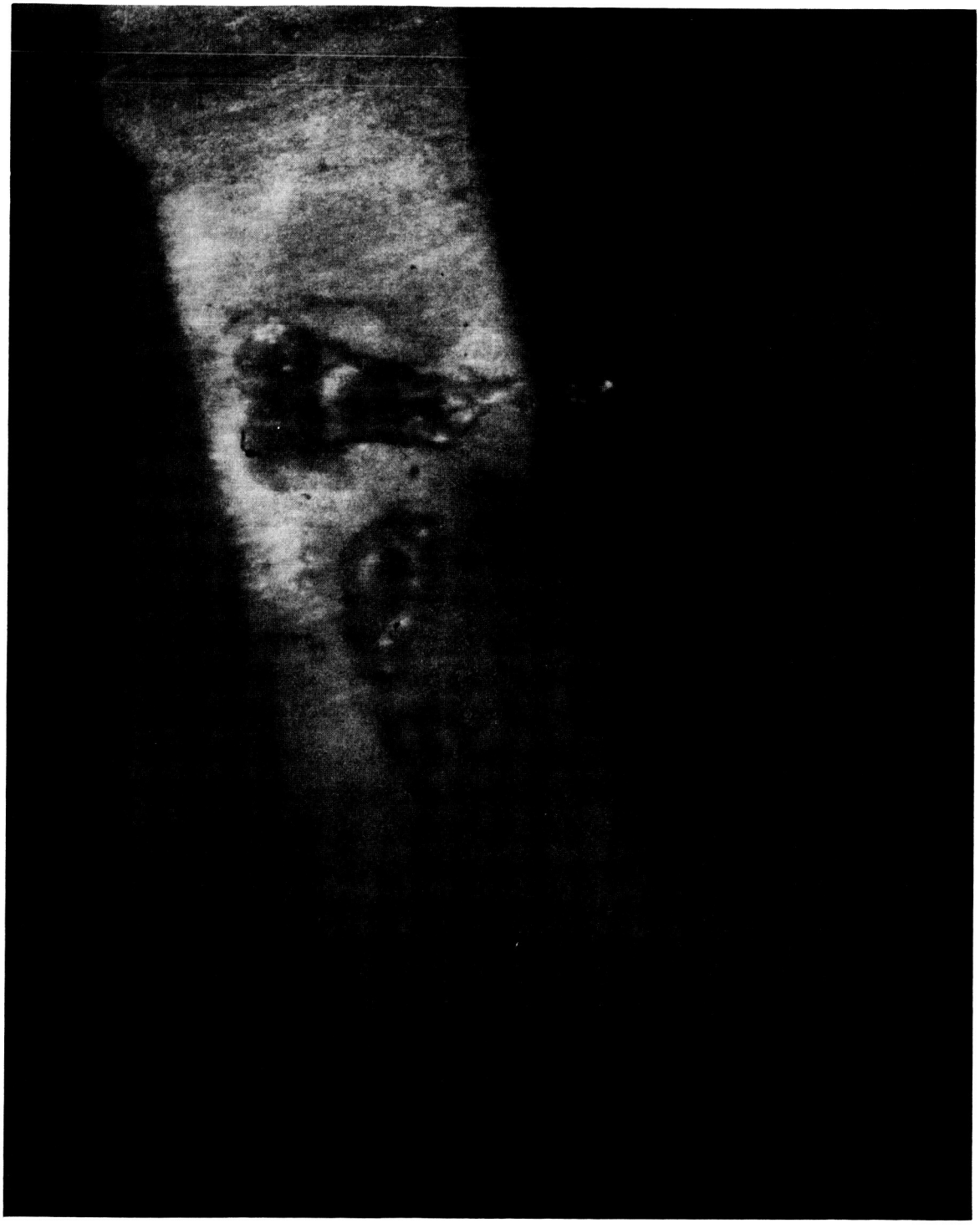

Figure 15. Drops Stripped from Puddle

which quickly breaks up into small drops. Frequently the stripping appears to be in sheets which immediately break into many drops of about the same size. The tongue and neck type of stripping is characteristic of the "primary" atomization described by Westinghouse (Ref. 8).

After the initial breakup, the drops are accelerated rapidly, apparently without further disintegration. The size of the droplets in Fig. 15 is 50 to 100 microns, which is typical of all the drops measured at 1200 ft/sec. This agrees well with the previous estimate of 60 microns based on the critical Weber number criterion used by Gardner (Ref. 3) as shown in Fig. 16. The drops measured at 600 ft/sec vapor velocity were 100 to 270 microns in size which also agrees well with the Weber number prediction of 230 microns.

Nozzle Test Loop

The test results obtained were subsequently confirmed and expanded in nozzle tests. Results were also obtained comparing water injection and turbine expansion as methods of obtaining wet vapor. With injection, a metered amount of water is injected into the turbine inlet line at the throat of a venturi; with expansion, the steam is passed through a turbopump where work is extracted to produce wetness. Figure 17 shows the test loop with the injection venturi attached to the test chamber. The alternate connection to the expansion turbine is also shown. The bypass from the expansion turbine (exhausting directly to the condenser) is used to control the inlet pressure to the test chamber while allowing sufficient flow through the expansion turbine to produce good efficiency and a high degree of wetness. The test chamber is the same as that used previously in the preliminary nozzle tests.

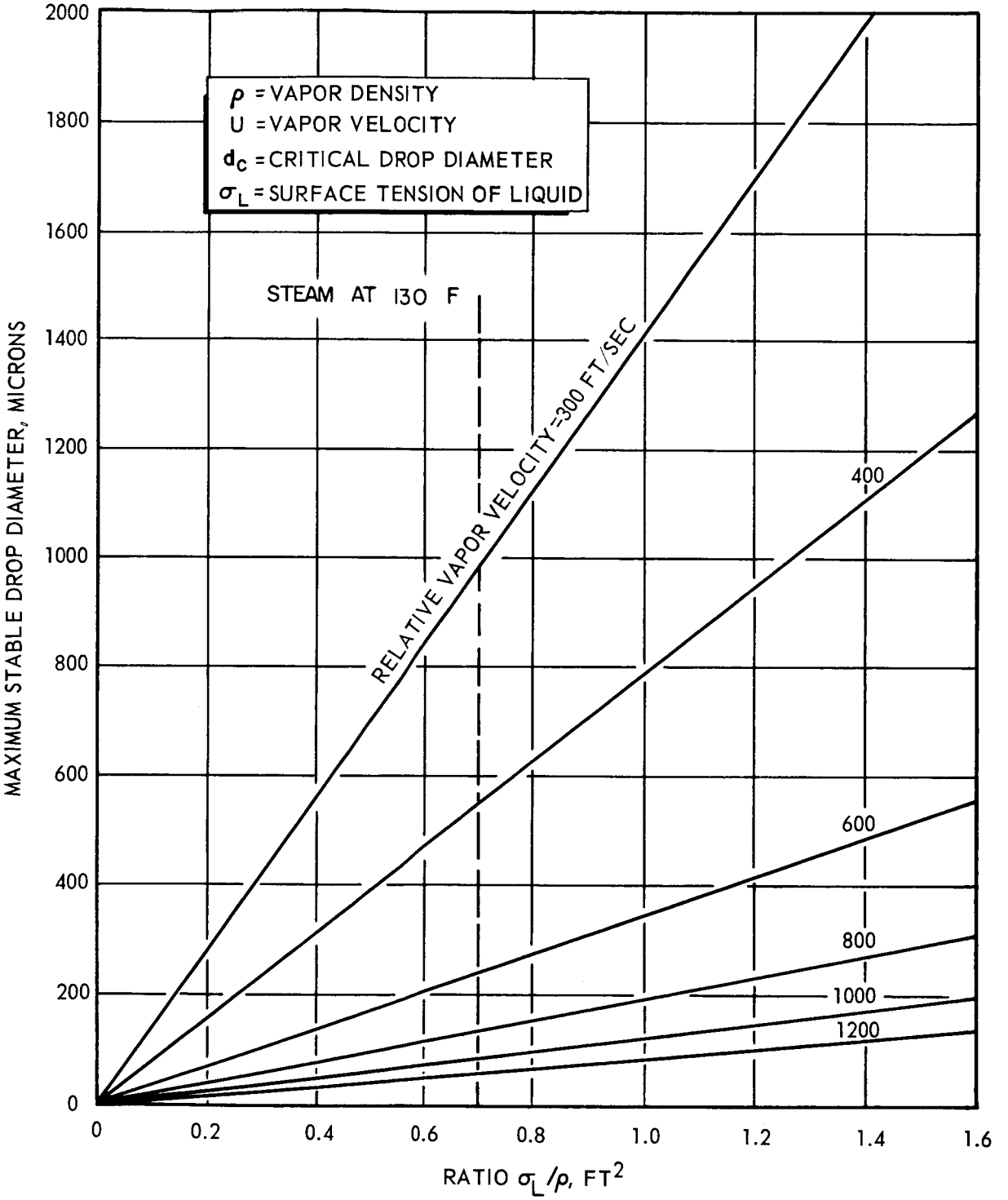

Figure 16. Maximum Stable Drop Diameter vs Surface Tension to Vapor Density Ratio (To Satisfy Critical Weber No. We = $\rho U^2 d_c/\sigma_L$ = 13)

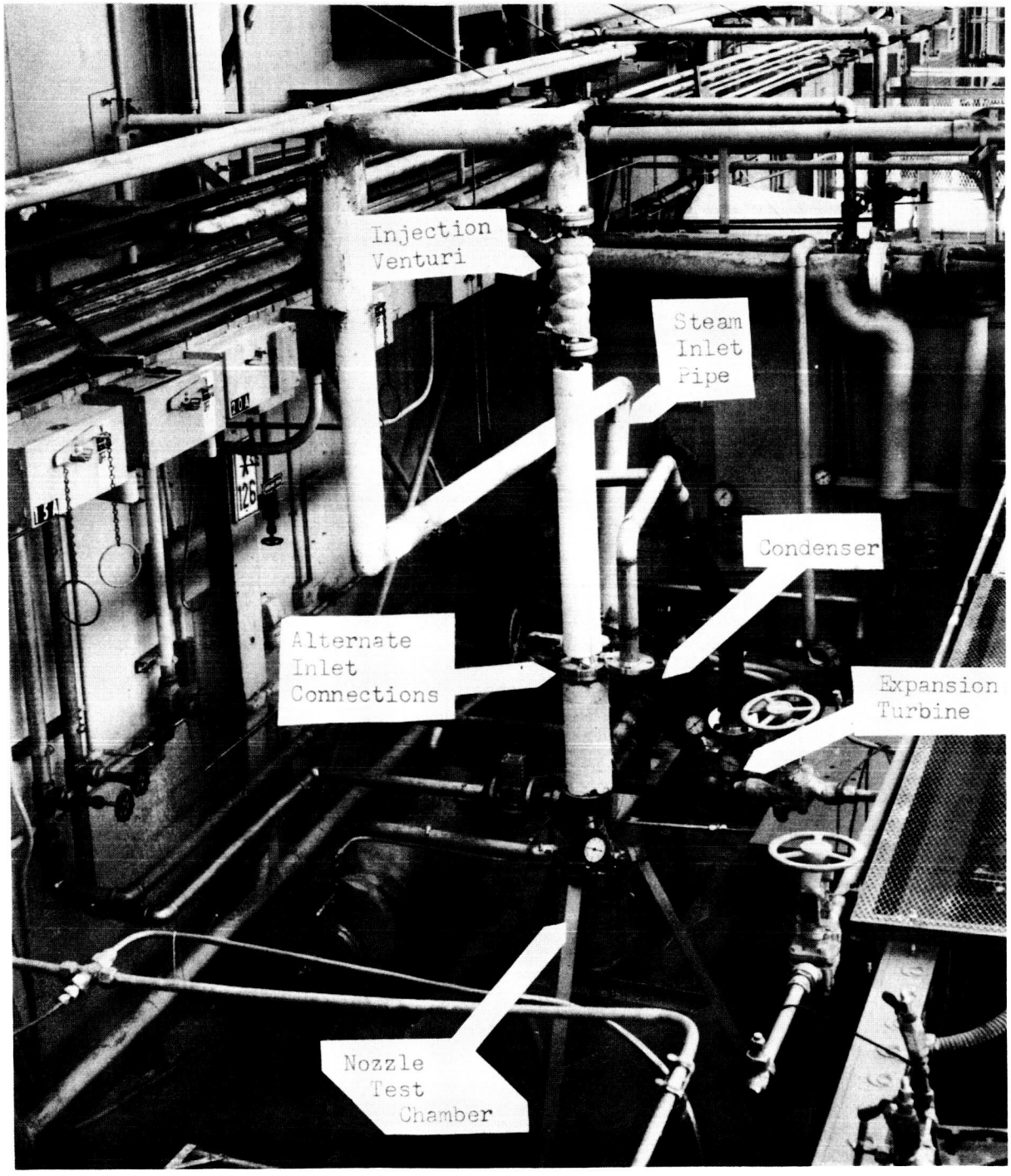

Figure 17. Turbine Erosion Program, Nozzle Test Facility

A wide range of test parameters were used to observe the different effects on moisture formation. Table 4 lists the range of conditions used and some of the reference conditions. As can be seen, the five conditions encompass the following matrix:

Condition	Pressure	Velocity	Moisture
1	Low	High	High
2	Low	High	Low
3	Low	Low	High
4	High	High	High
5	High	Low	High

In addition to the tests indicated in Table 4, tests were made using no injection at each condition as a reference.

Test data were obtained over the range of conditions indicated. Both high-speed (Fastax) and conventional (64 frames per second) motion pictures were obtained.

In general, the following observations apply:

1. With injection, large droplets are propagated through the nozzle ring. These are, quite probably, carried over from the inlet line where the moisture remains on the wall of the line. To observe this, a short transparent section was included just ahead of the test turbine inlet. Figure 18 shows short-duration still photos taken at this section during an injection test. Two types of conditions were observed; normally, steady streams of small drops propagated down the wall of the tube. Although

TABLE 4

SUMMARY OF TEST CONDITIONS

	Condition Number				
	1	2	3	4	5
Inlet Pressure, psia	4.5	4.5	2.8	9.6	6.2
Exhaust Pressure, psia	2.3	2.3	2.26	5.0	5.0
Inlet Moisture, Percent	8.3	4.0	10.1	8.2	10.1
Exhaust Moisture, Percent	11.0	7.0	11.0	11.0	11.0
Steam Velocity, ft/sec	1438	1450	807	1433	807

Normal

Intermittent
Streams

Figure 18. Inlet Distribution

it is not evident from the photograph, observations made during the test showed virtually no visible drops in the stream itself. Periodically, small rivulets (shown in the lower portion of Fig. 18) were observed. Simultaneously with their passage, droplet activity in the nozzle was greatly increased showing the correlation between water carryover and droplet shedding.

2. It is usual to find a fairly large puddle on the trailing edge of the nozzles. Figure 14 shows the puddle, which oscillates at an approximate period of 0.010 seconds, and sheds droplets in a manner very similar to that predicted by Pouchot (Ref. 8) and labeled sheet atomization. It must be noted that no sheet is evident on the suction surface as postulated by Pouchot.

3. A puddle is sometimes observed on the suction surface. This can be seen in Fig. 19. The exact reason for the existence of this puddle is not known but the fact that it does exist is evidence that it may be related to a region of separation. The separation may be due to the shape of the test assembly and/or off-design flow conditions.

4. With turbine expansion, drops approximately 400 microns in diameter can be seen moving down the suction surface. The drops move in the same track and show conclusively that no sheet formation is sustained. Droplet motion, as observed on the Vanguard Motion Analyzer, is shown in Fig. 20. The actual velocity of the drops (viewed axially) as the trailing edge is approached is only about 1 inch per second while the free stream velocity is in excess of 1000 feet per second. Once the drop passes the edge of the blade, it accelerates very rapidly.

5. It appears somewhat unusual that water drops should propagate over a stainless steel surface as very distinct, round drops, somewhat like drops on a non-wetting surface. Good wetting

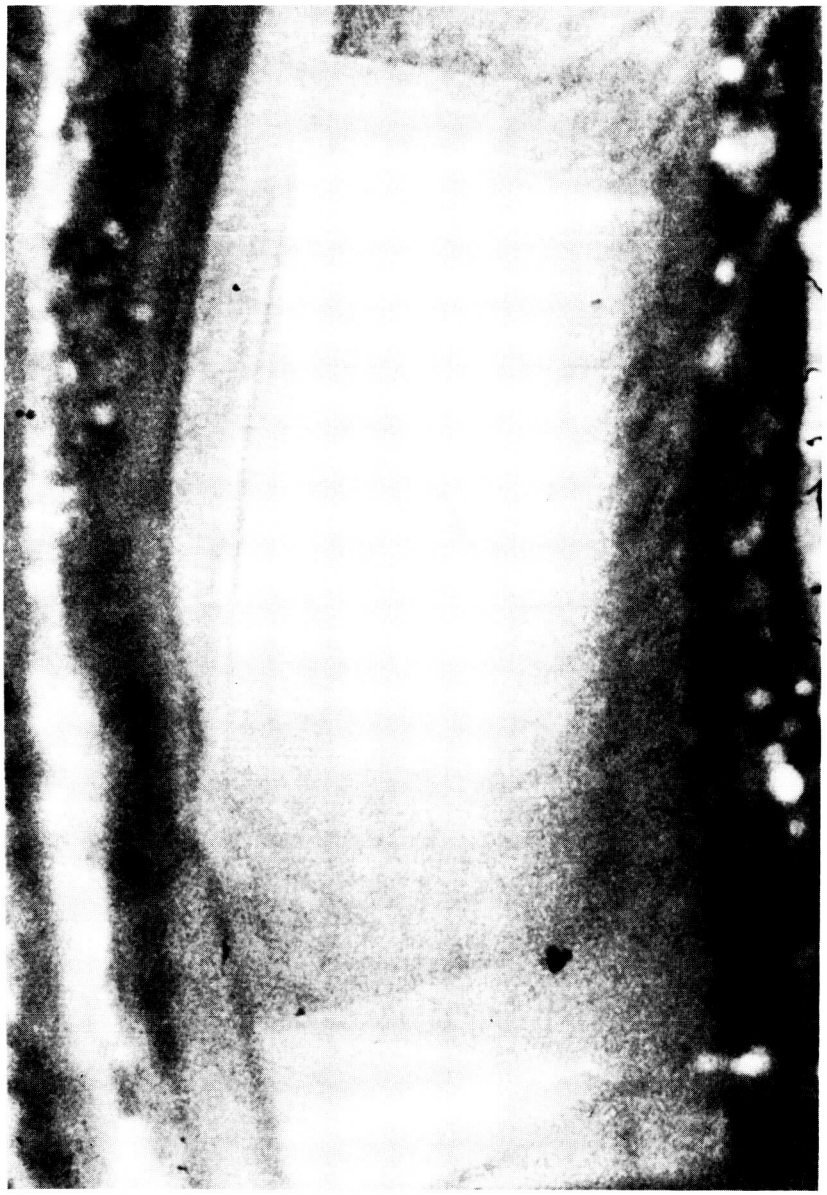

Figure 19. Accumulation on Suction Surface

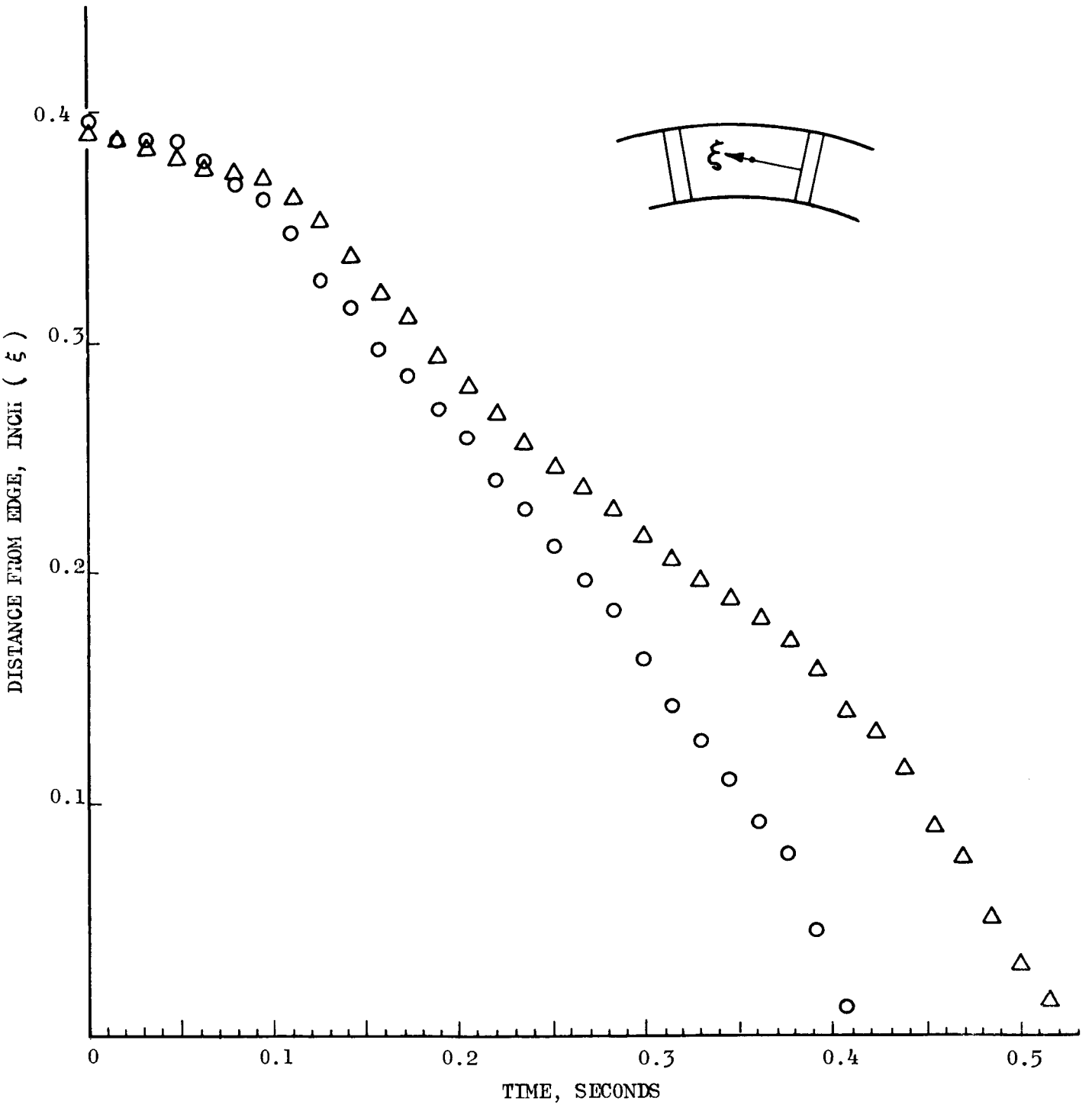

Figure 20. Path of Droplets on Suction Surface

would be expected, and this led to an investigation of the conditions involved. The surfaces had been thoroughly cleaned with acetone and distilled water to ensure that no oil film would effect the results. A supplemental experiment was made to determine the nature of these observations. Using the nozzle block, a drop of water was placed on the blade and found to spread as expected. With a stream of air, the drop was torn up and little distinct drops were dragged over the blade. The formation of the drops is, therefore, a function of the mechanics of flow, and sheet atomization is not observed.

Details of the droplet shedding process can be observed in Fig. 21 which shows 16 consecutive frames of a Fastax motion picture encompassing a duration of 0.0075 seconds. The puddle on the trailing edge oscillates and a finger of fluid moves out. The droplet detaches in Frame 8 and accelerates through Frames 9, 10, and 11 and is out of view in Frame 12 as the finger moves to the side. A second droplet detaches in Frame 11 as the finger recedes and the oscillation recurs. Droplet diameter is approximately 850 microns.

Evaluation of Tests

The results of the nozzle tests confirmed the sizes of the droplets to be observed and showed that Fastax photography could be used to observe the drops. It was also shown that puddles of considerable size were found on the walls of the stator and that these generated drops which would impact on the stator with considerable force because of their large size and low velocity.

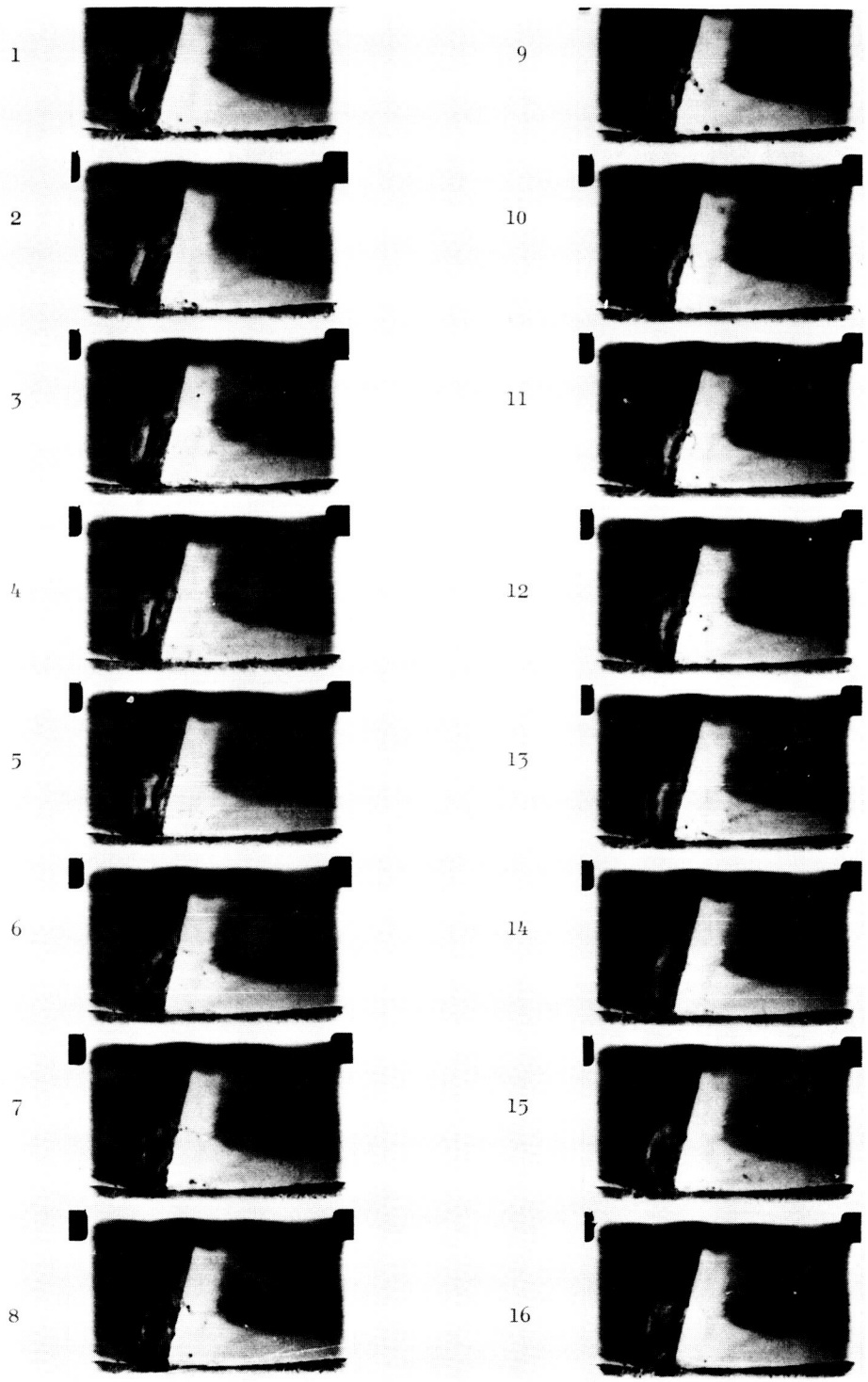

Figure 21. Droplets Leaving Trailing Edge of Web

The size of the droplet predicted for four conditions: We = 13, We/Re 1/2 = 1, WeRe = 4000, and Re = 380, is shown in Fig. 22 together with typical measured data points. The order of magnitude of the drops is confirmed although there is little indication which of the theoretical curves is correct.

TURBINE TESTS

The initial tests using the Fastax camera showed that droplets originating on the walls of the stator would lend themselves to photographic analysis. Provision had to be made in the test rig to provide proper lighting and viewing. Droplets moving with the stream, or the impact on blades moving at high velocity (800 ft/sec) could not be observed, of course. Ultra-high-speed photographic techniques using a Beckman and Whittley high-framing rate camera were investigated. Both laser pulsing and Xenon light sources were considered. The laser technique is the faster of the two, permitting exposure times down to 10 nanoseconds while the Xenon system is limited to approximately 40 nanoseconds.

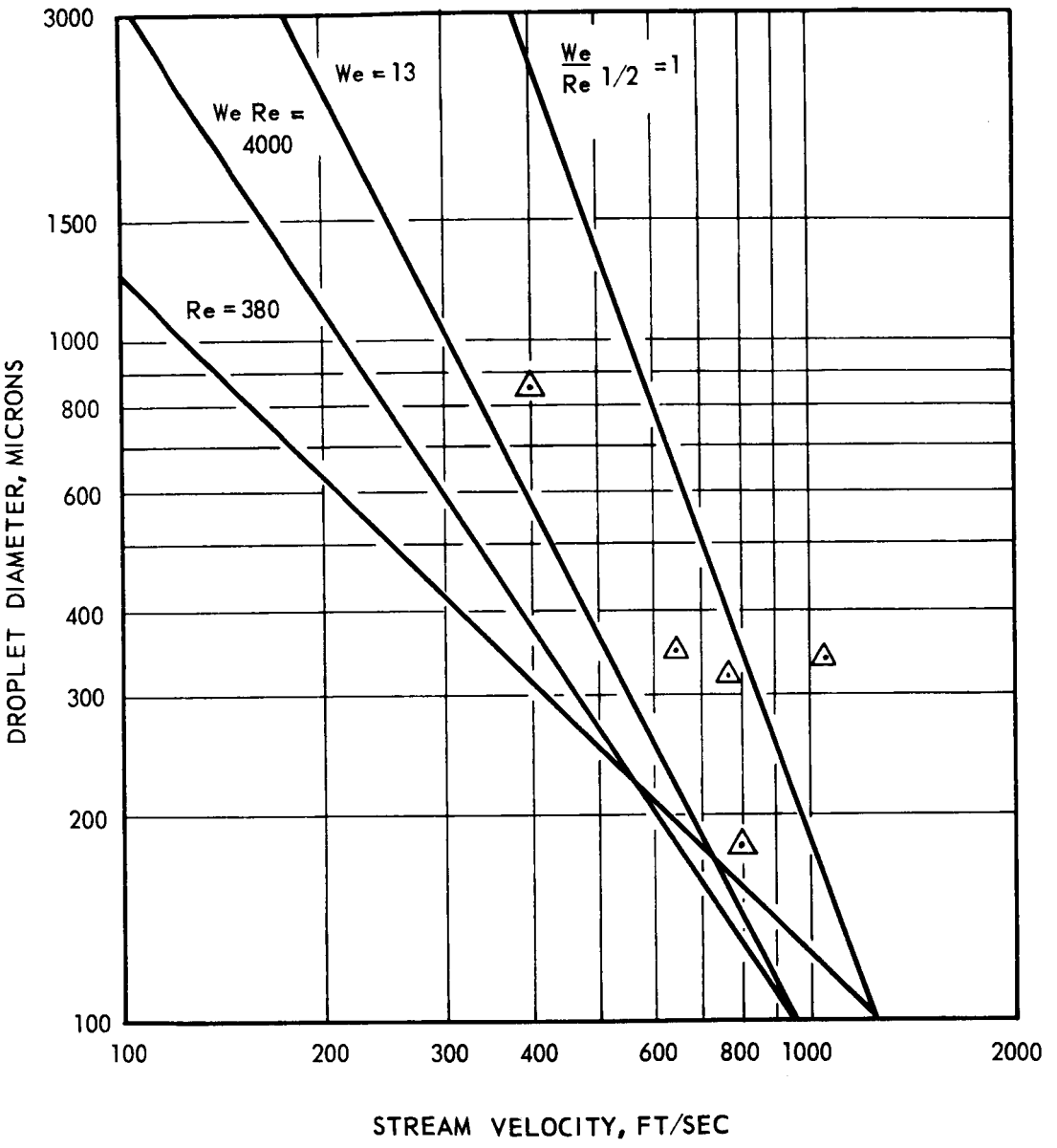

Figure 22. Critical Drop Sizes

FABRICATION OF TURBINE WHEEL

MATERIAL SELECTION

To study the material properties which may effect the erosion process, tests were planned using four materials under identical conditions. This involved the use of demountable blades so that all four materials could be used at the same time, and so that select blades could be changed to determine the effects of changing steam conditions.

The initial considerations depended on the selection of materials which would show erosion in a reasonable time period, which would span a range of material properties, and which would have sufficient strength to permit safe operation. Original correlation was based on a modification to the single-impact threshold velocity given by Engel (Ref. 9). Later considerations showed that this equation may yield velocities which are too high. The simple water-hammer equation was adopted as a design criterion. As shown in Ref. 10, the total pressure rise at the solid surface caused by an impacting drop is

$$\rho C V_i$$

where

ρ = density of fluid, slugs/ft^3
C = sound velocity in the fluid, ft/sec
V_i = impact velocity, ft/sec

Under repeated impact, the metal may be expected to fail when a sufficient number of cycles have been encountered at the impact stress, or

$$V_i = \frac{S_F}{\rho C}$$

where S_F = fatigue endurance limit, psi

On this basis, the threshold velocity (ft/sec) for various materials in steam is:

Haynes 25	1060
K Monel	700
AISI 316 Steel	590
10% Aluminum Bronze	340
Tens-50 Aluminum	310
Pure Copper (unannealed)	280
Pure Aluminum (2S-0)	200
Pure Aluminum (annealed)	81
Pure Nickel (annealed)	280
Pure Tantalum (annealed)	310
Pure Molybdenum (annealed)	470

The maximum allowable tip speed based on stress considerations was also calculated. On this basis, it was decided to fabricate blades of pure aluminum, pure copper, Tens-50 aluminum and AISI 316 steel. The pure aluminum would demonstrate whether or not damage can be obtained at low speed; the pure copper and Tens-50 aluminum have nearly equal threshold velocities; and the steel would afford a direct comparison to later potassium tests. Limiting turbine speed is 800 ft/sec.

FABRICATION OF BLADES

As discussed above, blades made of pure copper, pure aluminum, high-strength aluminum, and stainless steel were selected for inclusion in the test turbine. To make these blades demountable, a blade with a fir tree root was chosen. The design of this root section is a Rocketdyne standard which makes it possible to reduce blade costs by using existing broaches and grinding wheels. Blade profiles were cast to a predetermined shape which was adapted from a design for the flow of superheated 1600 F potassium. Detailed design was based on flow parameters developed and used at Rocketdyne on a previous program and took into account the low Reynolds number encountered (Ref. 11). The root section was ground to provide a fit in the broached turbine wheel which is made from a Waspalloy forging. Figure 4 shows the first- and second-stage wheels. Waspalloy was chosen for the wheel material so that the wheels could be used in the future in a potassium environment.

The casting process does not produce as smooth a finish on the blades as might be desired. However, casting is frequently employed in prototype systems and is, therefore, a realistic fabrication method. For measurement of erosion effects, the irregularities served as possible damage centers and observation of their influence was felt to be instructive. The irregularities appear to have had no effect (beneficial or detrimental) on erosion.

TESTING

The tests conducted to observe the droplets propagating through the stator block were described in the section dealing with the measurement aparatus In this section the tests using the special two-stage turbine will be described. These tests are currently being conducted. Evaluation and analysis of the results will be given in the next section.

TEST SETUP

Both the test rig and the test loop were described previously The blades and their method of fabrication were also discussed.

TEST OBJECTIVES

The objective of the test program was to subject blades made of four materials to the identical test conditions. This was done by placing replaceable blades on one wheel. In this way, all blades were exposed on equal amounts of time to each of the preset conditions.

STATUS

The test program is currently under way. Initial checkout tests were completed using the copper, Tens-50 aluminum, and stainless-steel blades. A coordinated series of seven 25-hour tests is now being conducted to determine the effects of tip speed, wetness, and spacing on the erosion of the blades. Data on weight loss are being obtained and are being evaluated. Correlation with material properties is under way.

TEST SEQUENCE

Checkout Test

A wheel using copper, Tens-50 aluminum, and stainless steel blades was operated in a checkout test where each of the blades was exposed to a variety of conditions. Table 5 shows the conditions used. The wheel is composed of 42 blades, so that 14 blades of each material were included. For balancing purposes, the blades were placed in groups of seven. Table 6 shows the weight of each blade before and after the accumulated test time shown in Table 5. Damage incurred by the aluminum blades is very consistent, with the spread in weight loss being limited to a relatively narrow range as indicated. The apparent weight gain in copper is attributed to surface oxidation.

During the checkout test, the impact velocity of the water drops hitting the moving blade was 240 ft/sec which is in excess of the calculated threshold velocity for pure aluminum (81 ft/sec). In this case, erosion is to be expected. For the Tens-50 aluminum, the calculated threshold velocity is 310 ft/sec. The average impact velocity for the 12 hours of operation above 10,000 rpm was approximately 285 ft/sec. Because erosion was observed, the calculated threshold velocity may be high due to variations in material properties, or the estimated impact velocity is low.

Figures 23, 24 and 25 show pictures of typical blades of each material taken before and after the test. In each case, the blades are magnified approximately six times. The casting process produces some roughness on the blade surface. It is interesting to note that erosion does not appear to be related to the irregularities in the surface. The damaged area is very sharply defined on the aluminum blades, but the stainless steel and copper blades show no damage. This, of course, correlates

TABLE 5

SUMMARY OF TEST CONDITIONS CHECKOUT TEST

Date, 1966	Duration, hr/min	Tip Speed, fps	Speed, rpm	Estimated Maximum Impact Velocity, fps	Pressure, in. Hg absolute	
					Inlet	Outlet
23 Sept.	0/20	144	5,400	120	10.8	8.5
26 Sept.	1/0	160	6,000	140	10.8	8.5
27 Sept.	4/25	181	6,800	150	10.8	8.5
28 Sept.	0/30	319	12,000	290	10.8	8.5
29 Sept.	2/5	239 to 385	9,000 to 14,500	335	8.0	3.0
30 Sept.	1/55	231	8,700	190	13.0	8.0
4 Oct.	2/50	335	12,600	295	19.0	13.0
5 Oct.	2/15	335	12,600	295	19.0	13.0
6 Oct.	4/10	280	10,500	255	19.0	14.0
Total	19/30					

TABLE 6

WEIGHT DATA FOR BLADES CHECKOUT TEST

Blade Number	Material	Weight, grams		Weight Change, milligram
		Start	Finish	
1	316	10.3000	10.2999	-0.1
2	316	10.4232	10.4232	0
3	316	10.3925	10.3924	-0.1
4	316	10.4046	10.4044	-0.2
5	316	10.5219	10.5218	-0.1
6	316	10.4344	10.4341	-0.3
7	316	10.4233	10.4235	+0.2
8	Copper	11.5780	11.5785	+0.5
9	Copper	11.6776	11.6427	*
10	Copper	11.6687	11.6692	+0.5
11	Copper	11.7235	11.7239	+0.4
12	Copper	11.5464	11.5467	+0.3
13	Copper	11.6160	11.6169	+0.9
14	Copper	11.8291	11.8294	+0.3
15	T-50	3.5353	3.5267	-8.6
16	T-50	3.6289	3.6035	*
17	T-50	3.5571	3.5483	-8.8
18	T-50	3.5735	3.5641	-9.4
19	T-50	3.5664	3.5577	-8.7
20	T-50	3.5430	3.5343	-8.7
21	T-50	3.6070	3.5981	-8.9
22	316	10.5348	10.5348	0
23	316	10.4468	10.4468	0

TABLE 6
(Concluded)

Blade Number	Material	Weight, grams		Weight Change, milligram
		Start	Finish	
24	316	10.5623	10.5622	-0.1
25	316	10.4577	10.4578	+0.1
26	316	10.6560	10.6560	0
27	316	10.4905	10.4905	0
28	316	10.5853	10.5855	+0.2
29	Copper	11.7059	11.7067	+0.8
30	Copper	11.4189	11.4193	+0.4
31	Copper	11.8146	11.8151	+0.5
32	Copper	11.7076	11.7083	+0.7
33	Copper	11.7272	11.7280	+0.8
34	Copper	11.7909	11.7918	+0.9
35	Copper	11.6216	11.6226	+1.0
36	T-50	3.5928	3.5850	-7.8
37	T-50	3.6104	3.6026	-7.8
38	T-50	3.6038	3.5940	-9.8
39	T-50	3.5898	3.5799	-9.9
40	T-50	3.5705	3.5610	-9.5
41	T-50	3.5831	3.5742	-8.9
42	T-50	3.6297	3.6119	*

AVERAGES

316	10.4738	10.4738	0
Copper	11.6730	11.6736	+0.6
T-50	3.5777	3.5688	-8.9

*Blade required clearance grinding during installation

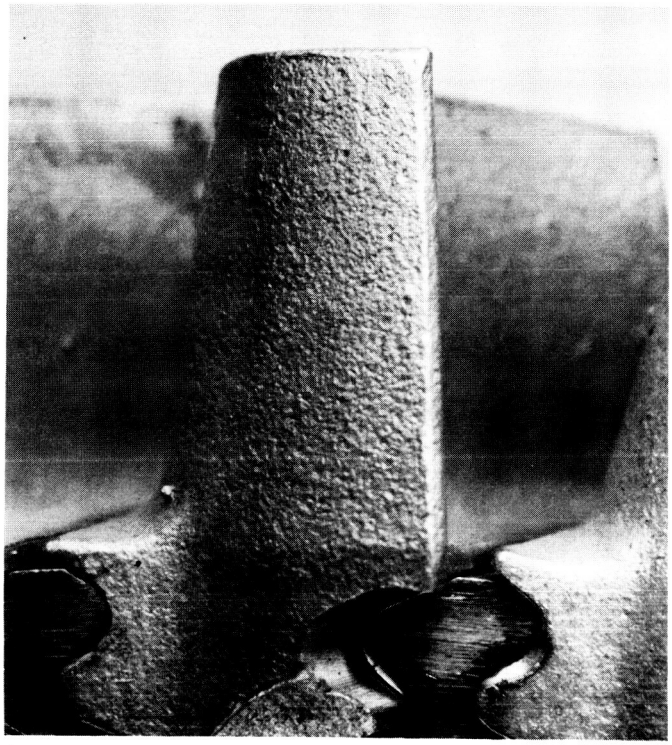

0.1 in.

Scale
(Approximate)

Before

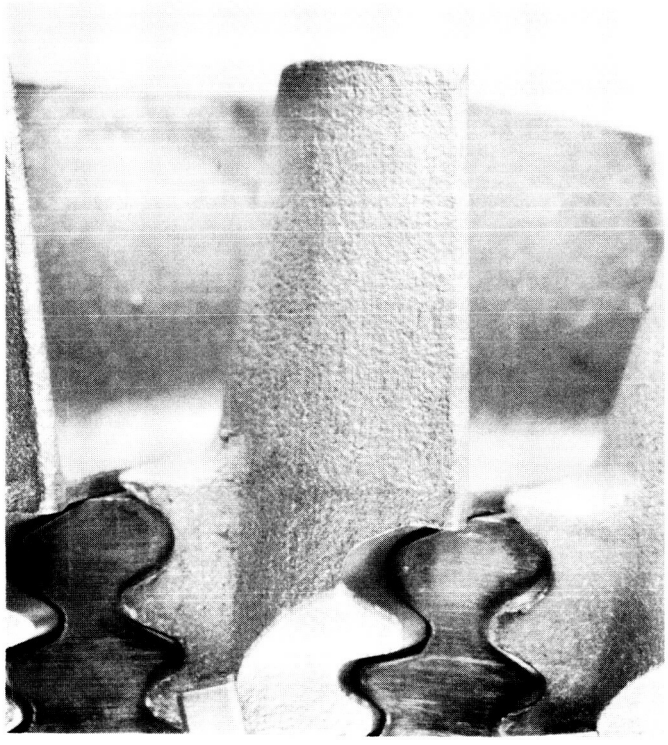

After

Figure 23. Stainless Steel Blade, No. 4, Checkout Test

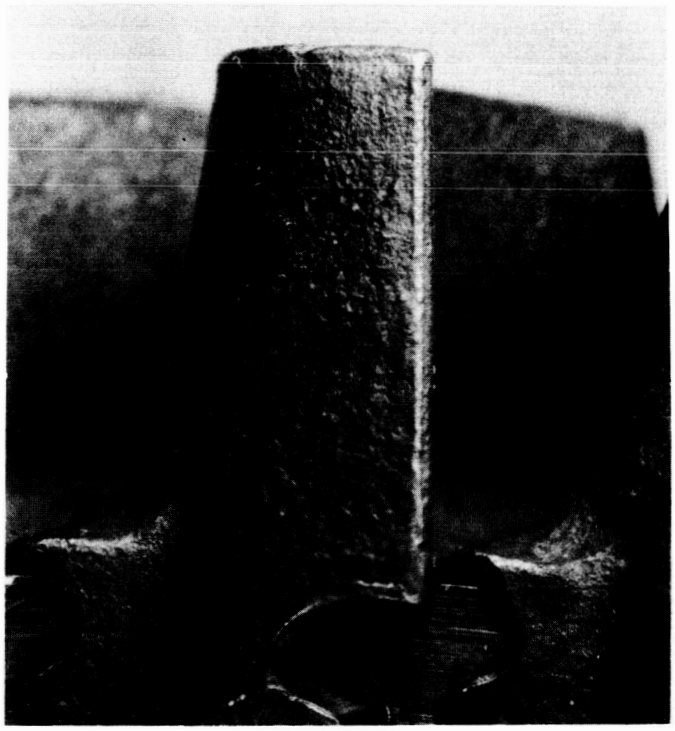

0.1 in.

Scale
(Approximate)

Before

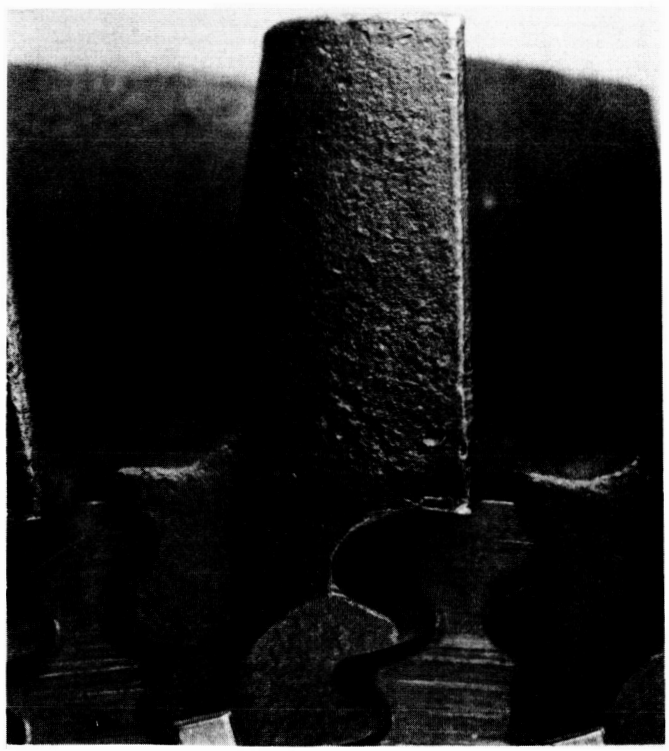

After

Figure 24. Pure Copper Blade, No. 11, Checkout Test

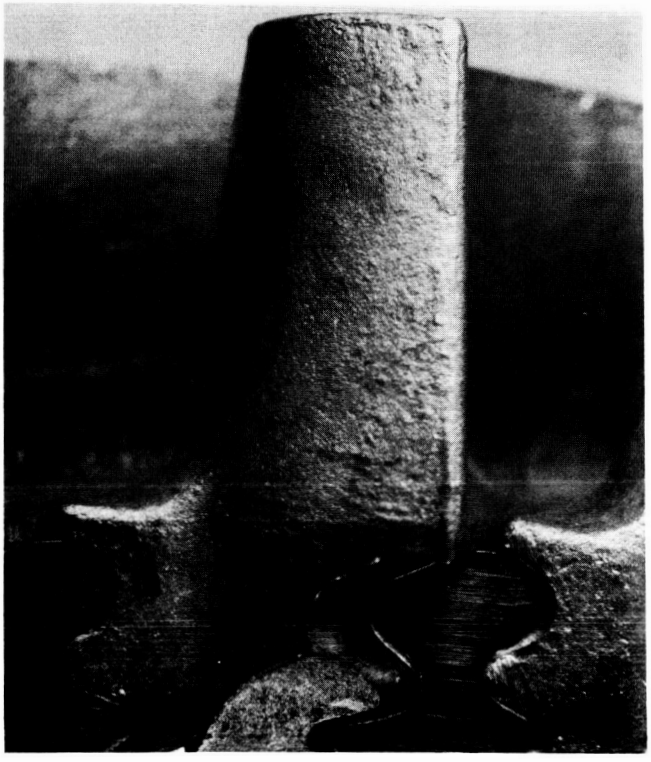

Before

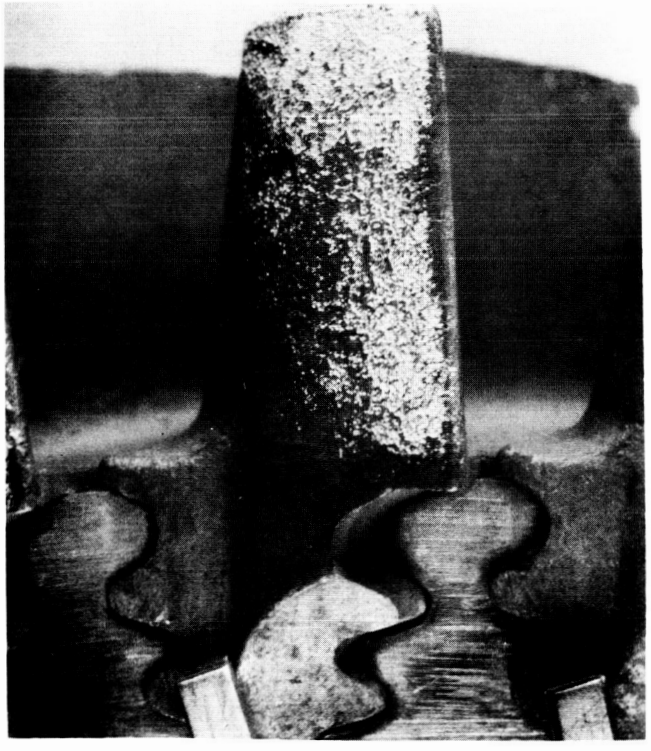

After

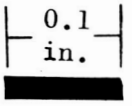

Scale
(Approximate)

Figure 25. Tens-50 Aluminum Blade, No. 39, Checkout Test

with the data in Table 6. The area of damage is uniformly distributed over the blade length except for the tip where excessive damage might be expected because of carryover on the walls of the throwoff from the previous stage.

To analyze the erosion patterns, Fastax pictures were taken through the window in the turbine housing (see Fig. 2) to observe the water droplet path. Droplet streamers were observed passing through the stator. These streamers are about 1000 microns in width and the drops resulting from their eventual breakup are 340 microns in diameter.

The checkout tests showed that erosion would take place after wet operation, but because no particular test condition was maintained, only comparative qualitative evaluation was possible. A series of tests at constant conditions was therefore planned.

Quality and Speed Tests

In the initial checkout test, the four test materials were subjected to wet steam estimated to contain 5-percent moisture, at the test turbine inlet. Tip speeds and impact velocities were as shown in Table 5. The velocities are above the threshold speed for pure aluminum (81 fps) and near the threhold speed for Tens-50 aluminum (310 fps) and pure copper (280 fps). The impact velocity is considerably lower than the threshold speed for AISI 316 steel (590 ft/sec). Table 7 lists the weight of the blades. Figures 26, 27, 28, and 29 show typical blade surfaces before and after this and the subsequent test. The damage to the pure aluminum is very severe with deep ruts in evidence. The Tens-50 aluminum is also badly eroded, although the ruts do not appear. The copper and steel blades

TABLE 7

WEIGHT DATA FOR BLADES

Blade Number	Material	Weight, grams			Weight Change, milligrams	
		0 Hours	25 Hours	50 Hours	0 to 25 Hours	25 to 50 Hours
101	316	10.5124	10.5130	10.5134	+ 0.6	+ 0.4
102	316	10.5099	10.5104	10.5107	+ 0.5	+ 0.3
103	316	10.4235	10.4242	10.4242	+ 0.7	0
104	Aluminum	3.6643	3.6457		-18.6	
105	Aluminum	3.4452	3.4332		-12.0	
106	Aluminum	3.6314	3.6094		-22.0	
107	Aluminum	3.6689	3.6510		-17.9	
108	Copper	11.7400	11.7419		+ 1.9	
109	Copper	12.0542	12.0560		+ 1.8	
110	Copper	11.3167	11.3185	11.3189	+ 1.8	+ 0.4
111	Copper	11.6540	11.6564	11.6563	+ 1.4	- 0.1
112	Copper	11.6261	11.6283	11.6282	+ 2.2	- 0.1
113	Copper	11.5228	11.5246	11.5246	+ 2.2	0
114	Copper	11.8847	11.8869	11.8865	+ 2.2	- 0.4
115	T-50	3.6503	3.6103		*	
116	T-50	3.6361	3.6015		-34.6	
117	T-50	3.5948	3.5721	3.5599	-22.7	-12.2
118	T-50	3.4956	3.4659	3.4509	-29.7	-15.0
119	T-50	3.5736	3.5596	3.5504	-14.0	- 9.2
120	T-50	3.6036	3.5792	3.5675	-24.4	-11.7
121	T-50	3.6075	3.5887	3.5769	-18.8	-11.8
122	316	10.6555	10.6560	10.6563	+ 0.5	+ 0.3
123	316	10.6152	10.6161	10.6164	+ 0.9	+ 0.3
124	316	10.6131	10.6138	10.6140	+ 0.7	+ 0.2

TABLE 7
(Continued)

Blade Number	Material	Weight, grams			Weight Change, milligrams	
		0 Hours	25 Hours	50 Hours	0 to 25 Hours	25 to 50 Hours
125	Aluminum	3.5760	3.5623		-13.7	
126	Aluminum	3.5933	3.5690		-24.3	
127	Aluminum	3.5713	3.5456		-25.7	
128	Aluminum	3.5835	3.5658		-17.7	
129	Copper	11.9294	11.9315		+ 2.1	
130	Copper	11.7148	11.7167		+ 1.9	
131	Copper	11.5397	11.5414	11.5418	+ 1.7	+ 0.4
132	Copper	11.7912	11.7934	11.7932	+ 2.2	- 0.2
133	Copper	11.9600	11.9621	11.9623	+ 2.1	+ 0.2
134	Copper	12.1712	12.1731	12.1733	+ 1.9	+ 0.2
135	Copper	11.8290	11.8310	11.8311	+ 2.0	+ 0.1
136	T-50	3.5848	3.5611		-23.7	
137	T-50	3.6494	3.6253		-24.1	
138	T-50	3.6158	3.5963	3.5850	-19.5	-11.3
139	T-50	3.5882	3.5631	3.5510	-25.1	-12.1
140	T-50	3.6199	3.5910	3.5800	-28.9	-11.0
141	T-50	3.6246	3.5978	3.5868	-26.8	-11.0
142	T-50	3.3552	3.3358	3.3255	-19.4	-10.3
204	316		10.5452	10.5455		+ 0.3
205	316		10.4655	10.4654		- 0.1
206	316		10.6110	10.6112		+ 0.2
207	316		10.3680	10.3689		+ 0.1
208	Copper		11.9709	11.9240		*
209	Copper		11.3820	11.3820		0
215	T-50		3.6530	3.6419		-11.1
216	T-50		3.6523	3.6356		-16.7

TABLE 7
(Concluded)

Blade Number	Material	Weight, grams			Weight Change, milligrams	
		0 Hours	25 Hours	50 Hours	0 to 25 Hours	0 to 50 Hours
225	316		10.4923	10.4928		+ 0.5
226	316		10.6259	10.6263		+ 0.4
227	316		10.4241	10.4243		+ 0.2
228	316		10.4218	10.4221		+ 0.3
229	Copper		12.0304	12.0311		+ 0.7
230	Copper		11.7309	11.7311		+ 0.2
236	T-50		3.5878	3.5794		- 8.4
237	T-50		3.5923	3.5824		- 9.9
			Averages			
	316	10.5549	10.5555	10.5558	+ 0.6	+ 0.3
			10.5205	10.5208		+ 0.3
	Aluminum	3.5917	3.5727		-19.0	
	Copper	11.7667	11.7687		+ 2.0	
			11.7276	11.7277		+ 0.1
	T-50	3.5857	3.5606		-25.1	
			3.5667	3.5552		-11.5

* Blade required clearance grinding during installation

Figure 26. Stainless Steel Blade, No. 103

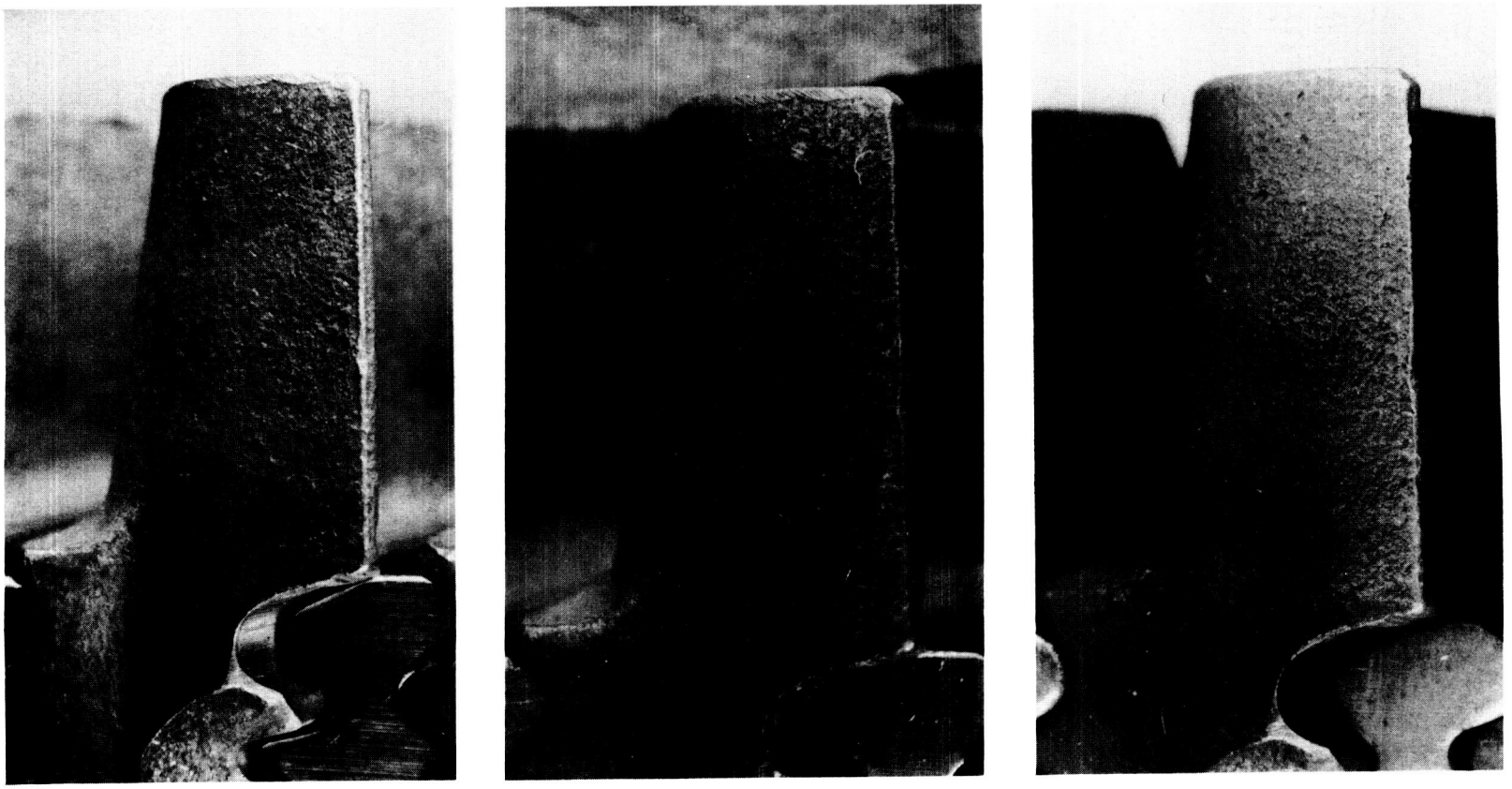

Figure 27. Copper Blade, No. 110

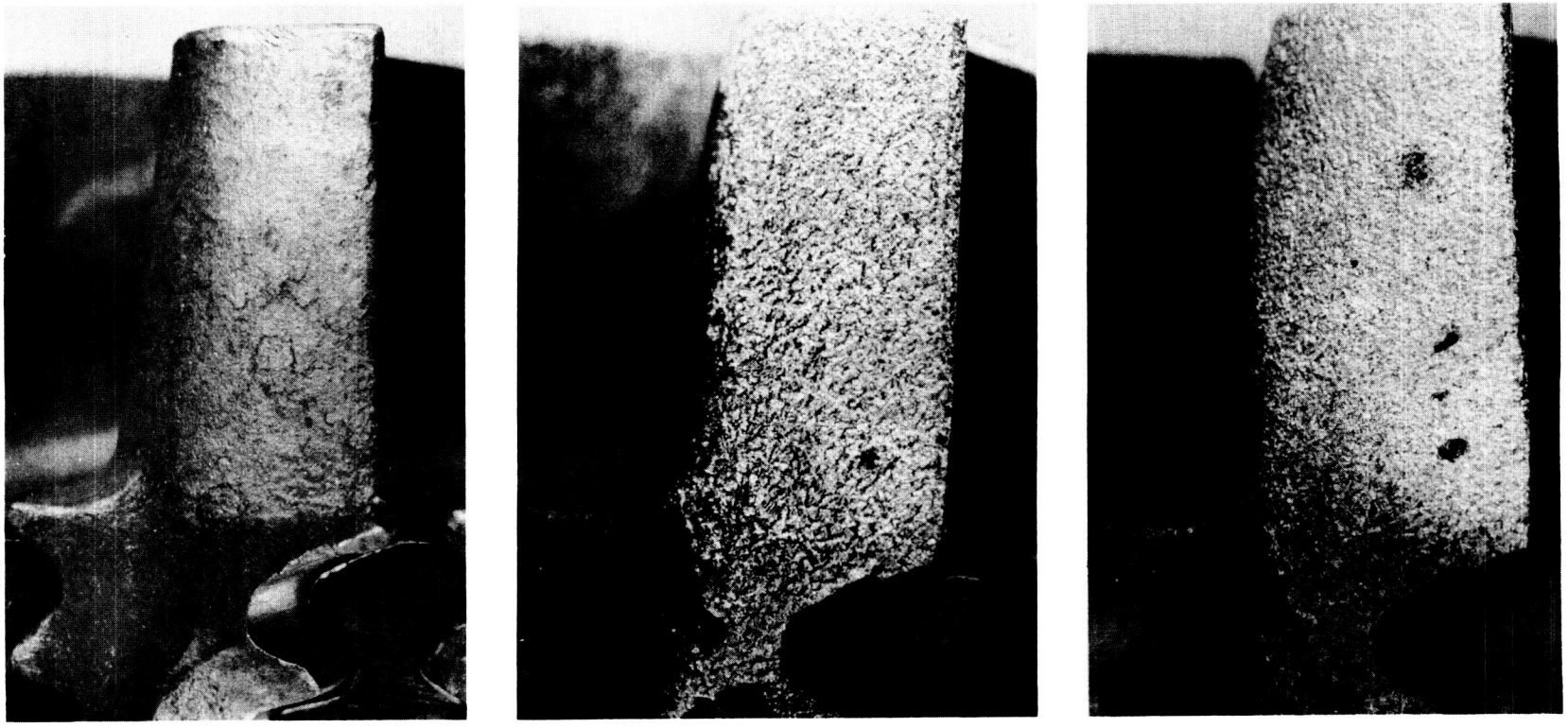

0 Hours

25 Hours

50 Hours

0.1 in.

Scale
(Approximate)

Figure 28. Tens-50 Aluminum Blade, No. 140

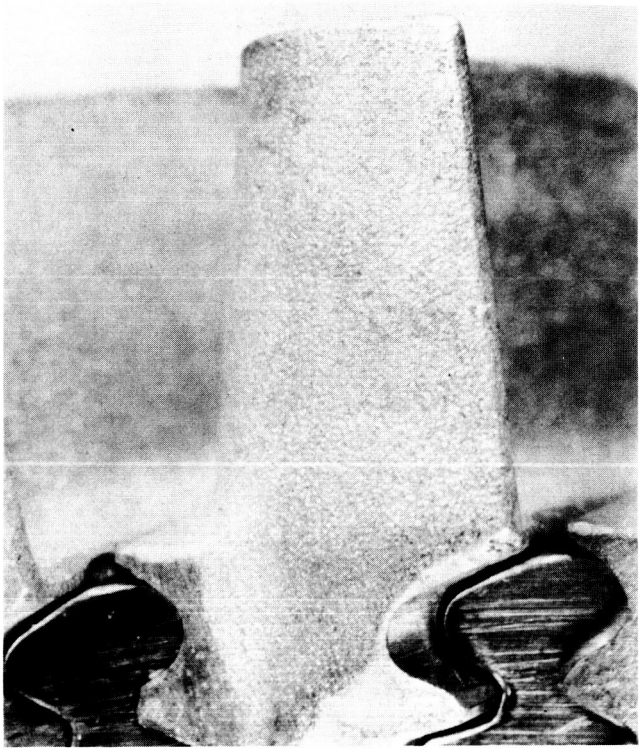

0.1 in.

Scale
(Approximate)

0 Hours

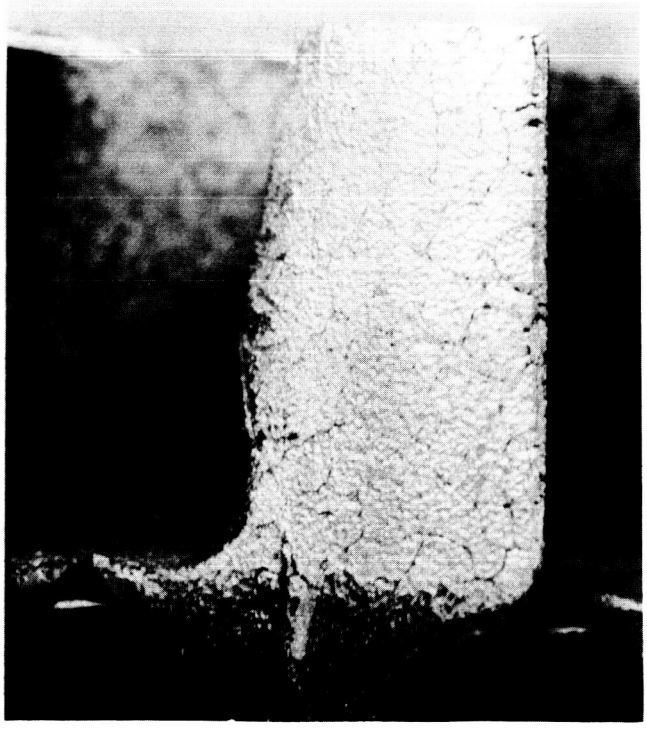

25 Hours

Figure 29. Aluminum Blade, No. 125

appear to be unaffected. Weight loss data are again very consistent and the copper shows another weight gain, probably caused by oxide formation. The composition of the materials is given in Appendix B.

Following the first 25-hour test, a second 25-hour test was begun. In this test, the quality was maintained the same as in the first test, and the tip speed increased to 460 ft/sec which is considerably above the calculated threshold speed for copper (280 ft/sec) and Tens-50 aluminum (310 ft/sec). No pure aluminum blades were used because the tip speed is above the safe operational limit for this material. The pure aluminum blades were replaced with steel blades, and four blades each of copper and Tens-50 aluminum were replaced to determine the effect of the higher speed on unexposed blades. In this way, a comparison based on cumulative impact can be made.

ANALYSIS

Evaluation and analysis of tests now in progress has not been completed. However, the results of those tests which have been performed makes it possible to evaluate the data and to draw some tentative conclusions.

DROP FORMATION

Nozzle Tests

The flow of a wet vapor through a stator block results in the formation of drops which move at less than stream velocity. These drops may have their origin in puddles which form on the web and the walls of the stator, in the low velocity wake and separation regions. Drops formed in a prior stage, or on housing walls will also contribute to the number of drops observed. The size of the drops is in the range of those predicted by the Weber number analysis, as shown in Fig. 22. Expansion of vapor through a prior stage appears to result in a more uniform flow with fewer drops on the stator walls, whereas with injection, streams of water flow along the housing walls. Because of the relatively small size of the blades in a space-power turbine, the distribution of the drops is not limited to the tip region, and damage over the whole leading-edge region may be expected.

Turbine Tests

The droplet formation observed in the nozzle tests was also observed in the turbine tests. With an inlet quality of approximately 98 percent to the test turbine, the expansion observed in the second stator shows a

large number of drops with streams of liquid flowing on walls. The nature of the flow is dependent on the pressure ratio and on the quality reached. Under some conditions, the physical location where spontaneous condensation begins can be observed.

MATERIAL EVALUATION

Based on analytical considerations using the water-hammer equation, the threshold velocity for the four materials being used was calculated to be:

AISI 316 Steel	590 ft/sec
Pure Copper	280 ft/sec
Pure Aluminum	81 ft/sec
Tens-50 Aluminum	310 ft/sec

Tests run so far have shown damage to occur to the two sets of aluminum blades at a tip velocity of 300 ft/sec, but no significant weight loss has been encountered for copper and steel at a tip speed of 460 ft/sec. At tip speeds of 700 ft/sec, some steel weight loss was observed. Copper was not run at this tip speed.

Examination of Fig. 26 through 29 shows that the aluminum damage is confined to a region along the pressure side extending about 0.2 inches back of the leading edge. At the tip, the damage line extends back further, nearly half the length of the blade. This tip erosion is to be expected because of drops being propagated along the housing wall. Some of these are, in all probability, the result of centrifugal action in the previous stage.

The clearly defined line of damage indicates that the moisture is evenly dispersed over the whole flow channel.*

The granular appearance of the aluminum blades is evidence of the dendritic structure of the metal. Even though the aluminum blades are "pure," a small amount of trace elements is present to facilite pouring, as shown in Appendix B (silicon 0.002, copper 0.003, magnesium 0.001, iron 0.003). Mechanical working of the surface may cause removal of the segregates, resulting in the appearance evident in the pictures.

Blade weight loss indicates very little, if any, erosion of the copper and steel blades. In the copper blades, no impurities were evident and the dendritic segregation is not be expected. The tip speeds used so far are, of course, below the threshold of the stainless steel.

The weight-loss data shown in Tables 6 and 7 indicates some key results. Essentially no change is evident on the steel blades. The copper blades increased a slight amount in weight during the first 25 hours, but not during the second test. Even the four copper blades which were placed in the system during the second test show little weight gain. Additional data will be obtained during the third test to evaluate this weight change.

Aluminum blades show relatively constant weight changes. During the first 25 hours, the pure aluminum blades lost an average of 19.0 milligrams which is the equivalent of 0.004-inches mean depth of layer removed over the affected area. The minimum weight loss was 12.0 milligrams and the maximum 25.7 milligrams, a spread of -27 and +28 percent. The Tens-50 aluminum blades lost an average of 25.1 milligrams (0.0055-inch mean depth of layer removed) with a spread of -44 and +38 percent. During the

*Estimates of the velocity of impact of various droplets based on the location of damage are given in Appendix D.

second test, the average loss for all Tens-50 blades was 11.5 milligrams, -27 and +45 percent. No significant difference seems to exist between these blades used only in the second test and those tested for the full 50 hours. The larger weight loss registered by the Tens-50 blades may be the result of the greater amount of alloying material in this metal.

The relatively large spread in blade weight listed in Tables 6 and 7 is attributable to the differences which naturally result from casting and the need to hand grind the platform section between the root and the blade during assembly. All blades were X-rayed prior to use to ensure no porosity or voids in the metal. The material density was also determined. Typical values are shown in Table 8 .

TABLE 8

SPECIFIC GRAVITY OF METALS

Material	Specific Gravity	
	Measured	Theoretical
AISI 316 Steel	7.963 7.955	7.98
Copper	8.914 8.729	8.96
Aluminum	2.630 2.639	2.67

Analysis and correlation of data is continuing.

LASER PULSING SYSTEM

To observe the passage of drops through the rotor stage, it is necessary to photograph at a speed which will effectively stop the action. Fastax camera sequences obtained in the nozzle tests had exposure times of 6 microseconds at a framing and pulsing rate of 5000 frames per second. In 6 microseconds, each blade moves approximately 0.060 inches, which would not permit a clear picture. Furthermore, at a framing rate of 5000 frames per second, each blade will rotate 1.8 inches between frames which would not permit analysis of drop paths, even if the framing rate were doubled (to the limit of the Fastax camera). A much faster system was, therefore, required.

For recording purposes, the use of a Beckman and Whitley camera was proposed early in the program. Such a camera is capable of framing rates up to 1.2-million frames per second, a rate which would stop the motion of the blades very effectively. Light shuttering is achieved by means of a rotating mirror which utilizes a Xenon light source.

A more effective way of utilizing the Beckman and Whitley camera was demonstrated by Ellis and Fourney and is described in Ref. 12. This method uses a laser which is pulsed and modulated by a Kerr cell to produce exposure times to 10 nanoseconds. A comparative evaluation of the laser and Xenon techniques was made. It was concluded that the laser system was more sophisticated and promised better results because the Xenon source would achieve 40-nanosecond exposures at best. It would also require extensive modification to the mirror system on the camera which would, in the long run, be no less expensive than adaption of an existing laser.

The laser pulsing system being used is an adaptation of that used by Prof. Ellis and was worked out in consultation with him. Two systems were considered as shown in block diagram form in Fig. 30. System 1 uses a commercially available 100 volt, 0 to 1 megacycle pulse generator; system 2 uses a 10 volt, 0 to 3 megacycle commercial pulse generator in conjunction with a Rocketdyne-constructed 10:1 intermediate pulse amplifier. While the first system is simpler, it is limited to 1-million flashes per second, while the second system can achieve 3-million flashes. System 2 was selected for construction. As indicated in the block diagram (Fig. 30), the generated pulse is amplified and used to activate a Kerr cell shutter. This shutter modulates a laser beam and an image is recorded on the Beckman and Whitley camera which is used as a streak camera.

The laser pulsing system has been checked out and is being installed in the test setup prior to taking pictures. The camera has been modified and operated to ensure an adequate field of view. Pictures will be taken during the remainder of the test program to attempt to observe the droplet velocity and impact on the turbine wheel.

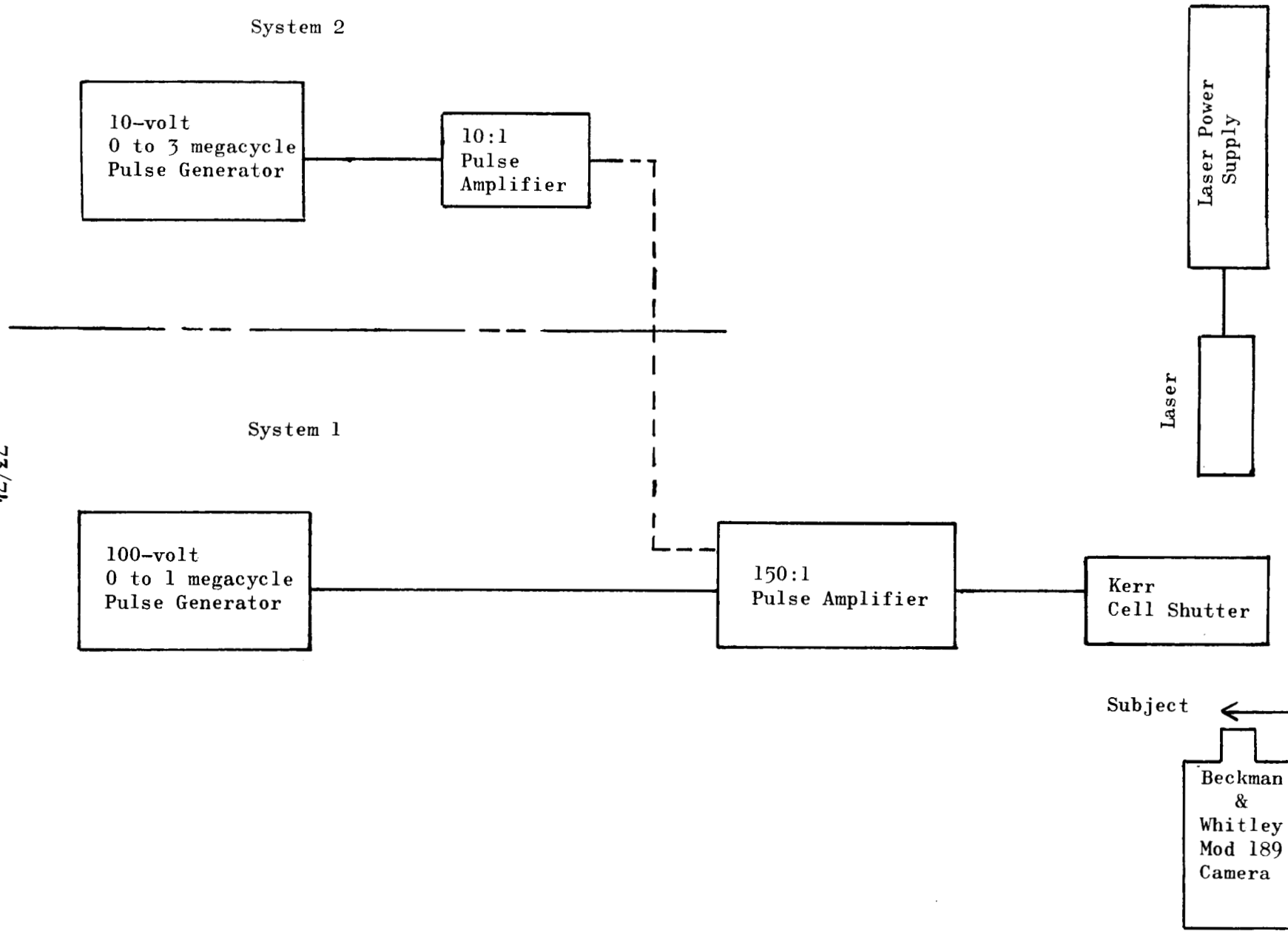

Figure 30. Laser Pulsing System Schematic

REFERENCES

1. Gyarmathy, G., and H. Meyer: "Spontaneous Condensation Phenomena-Parts I and II," VDI Forschungsheft 508 (1965), Translation by CEGB Information Services, C. E. Trans. 4160.

2. Hill, P. G., H. Witting, and E. P. Demetri: "Condensation of Metal Vapors During Rapid Expansion," Journal of Heat Transfer, November 1963, p. 303.

3. Gardner, G. C.: "Events Leading to Erosion in the Steam Turbine," Proc Instn Mech Engrs 1963-64, Vol. 178, Pt. 1, No. 23, p. 593.

4. Rabin, E., A. R. Schallenmuller, and R. B. Lawhead: Displacement and Shattering of Propellant Droplets, Rocketdyne, a Division of North American Aviation, Inc., R-2431 (AFOSR TR 60-75), Canoga Park, California, March 1960.

5. Wolfe, H. E., and W. H. Andersen: Kinetics Mechanism and Resultant Droplet Sizes of the Aerodynamic Breakup of Liquid Drops, Aerojet-General Corp., Report 0395-04(18)SP., April 1964.

6. Hanson, A. R., E. G. Domich, and H. S. Adams: "Shock Tube Investigation of the Breakup of Drops by Air Blasts," The Physics of Fluids, Vol. 6, No. 8, August 1963, p. 1070.

7. Hays, L.: Turbine Erosion Research in Great Britain, unpublished report, Jet Propulsion Laboratory, Pasadena, California.

8. WANL-PR-(DD)-006, Basic Investigation of Turbine Erosion Phenomena-Contract NAS7-390-November 1965 Progress Report, Westinghouse Astronuclear Laboratory.

9. Engel, O.G.: "Pits in Metals Caused by Collison With Liquid Drops and Soft Metal Spheres," NBS J. Res. 62, 6, 1959, 229-246.

10. WANL-PR(DD)-013, Basic Investigation of Turbine Erosion Phenomena-Contract NAS7-390-Amendment 1-Quarterly Progress Report, July through September 1966, Westinghouse Astronuclear Laboratory.

11. Binsley, R.L.: Aerodynamic Design of the Potassium Turbine, Nuclionics Division of Rocketdyne, NM-64-21, 15 July 1964.

12. Ellis, A. T. and M. E. Fourney: "Application of a Ruby Laser to High-Speed Photography," Proc of the IEEE, Vol. 51, No. 6, June 1965.

13. Dickerson, R. A. and T. A. Coultas: "Breakup of Droplets in an Accelerating Gas Flow," AIAA Paper No. 66-611, June 1966.

14. WANL-PR-(DD)-014, Analytical Investigation of Turbine Erosion Phenomena--Interim Technical Report Number 1, Volume 1, Contract NAS7-390, Westinghouse Astronuclear Laboratory, 1 November 1966.

APPENDIX A

SIMILARITY CONSIDERATIONS FOR DROPS

Much work has been published on the formation of drops in moving gas (vapor) streams. Two types of drops are recognized in a vapor system: those condensing in the stream, and those resulting from the agglomoration of the condensed drops. The former are very small (submicron) and their size is governed by thermodynamic conditions (e.g., heat transfer, see Ref. 1). The much larger, agglomorated drops are of interest here.

Available data comes from many sources; e.g., aerosol spray studies, rocket propellent distribution, droplets shattered by shock waves. Very little agreement can be found between the various reports. However, generally the Weber Number

$$We = \frac{\rho U^2 d}{\sigma}$$

and the Reynolds Number

$$Re = \frac{\rho U d}{\mu}$$

where

ρ = gas (vapor) density
U = relative velocity
d = droplet diameter
σ = droplet surface tension
μ = gas (vapor) viscosity

are used to correlate.

If the droplet is moving slowly relative to a gas system, the flow around the nearly spherical drop is laminar. The forces acting on the drop are proportional to the dynamic pressure around the drop and its characteristic area

$$F_d \alpha \frac{\rho U^2}{2} d^2$$

and the surface tension forces holding the drop together

$$F_{st} \alpha \sigma d$$

The critical drop size occurs when these forces are in some critical proportion.

$$\frac{\rho U^2 d^2}{2} = K \sigma d$$

where

K = constant

Evidently the Weber Number

$$We = \frac{\rho U^2 d}{\sigma} = 2K$$

is a constant in this case. This constant is quoted variously as being between 10 and 25 (e.g. Ref. 3 and 6).

As the relative velocity increases, the dynamic forces play a larger part; the drop may deform and surface waves may develop. Ref. 4 (among others) shows that the drop assumes a lenticular appearance and the surface friction forces come into play. Shear-type breakup is imminent when the sur-surface friction is large enough. In addition to the dynamic forces, the shear-type force must be opposed by surface tension. This force, too, is proportional to the dynamic pressure

$$F_f \alpha C_f \frac{\rho U^2}{2} d^2$$

In Ref. 4 it is shown that for laminar flow, C_f is proportional to $Re^{1/2}$ making

$$WeRe^{-1/2} = \text{constant}$$

As the slip velocity increases, turbulent flow is achieved about the drop. Classical theory shows that in the transition zone

$$C_f = \frac{K_1}{Re^{0.2}} - \frac{K_2}{Re}$$

The shape of this curve is such that the Reynolds number dependence varies from

$$C_f \alpha Re$$

at the beginning of transition to

$$C_f \alpha \frac{1}{Re^{0.2}}$$

when turbulence is achieved. At this point one might expect that

$$We Re^{-0.2} = \text{constant}$$

The droplet may also break up because of a shock-wave impingement. In this case, the drop is flattened until, at a critical velocity, the drop is blown out down stream, like a bag attached to a heavy rim. The bag finally bursts, producing many fine drops. This type of breakup, called bag-type breakup, must be governed by a different correlation. In Ref. 6 it is indicated that

$$We Re = \text{constant}$$

In the light of this discussion, it might be interesting to examine the data obtained by some investigators. In Ref. 7, Hays reports some data obtained from a turbine operated at CERL. The droplet velocity and size downstream of a blade-row are given for five conditions in a wet stream tunnel. Steam pressure is listed and from this, the steam density may be estimated. In essence, the density, surface tension, and velocity are the same for each series of points and so the plot of Reynold number vs Weber number is a 45-degree line. If all test conditions were known this would, probably, be changed. Figure 31 shows this graph. The relative velocity for each line is shown. In each can, the relevant equation is

$$\frac{We}{Re} = \text{constant}$$

but the constant appears to change with the velocity as follows:

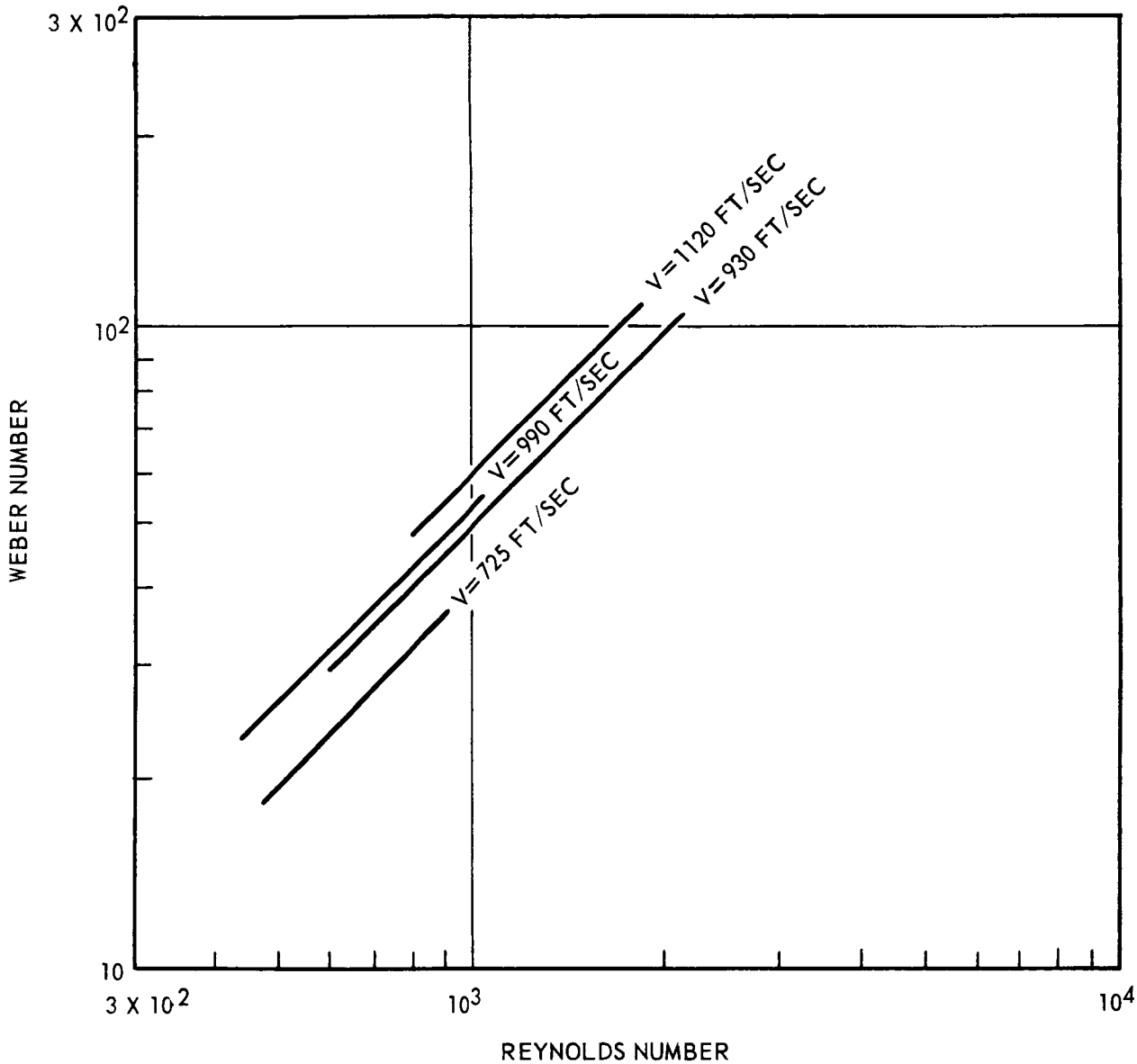

Figure 31. Critical Drop Size Correlation, Water in Steam, Data of Ref. 7

Velocity	Constant
725	0.039
930	0.049
990	0.052
1120	0.058

or

$$\text{constant} = 3.0 \times 10^{-4} \, (\text{velocity})^{0.75}$$

which would lead to the conclusion that

$$\frac{We}{Re} = 3.0 \times 10^{-4} \, V^{0.75}$$

This equation has, of course, dimensional units, but not enough data is available to proceed beyond this point.

In Ref. 13 the droplets breaking up in an accelerating air stream are investigated. Data are given for three fluids (water, glycerin, and methanol) and the droplet diameter just before breakup is correlated with Weber and Reynolds number. If these data are plotted as in Fig. 32, 33, and 34 the best fit line through each set of data yields an equation of the type

$$\frac{We}{Re^{1.2}} = \text{constant}$$

although the constant varies with density of gas and with fluid. For water and air density of 0.017 the constant is 1.12×10^{-2}.

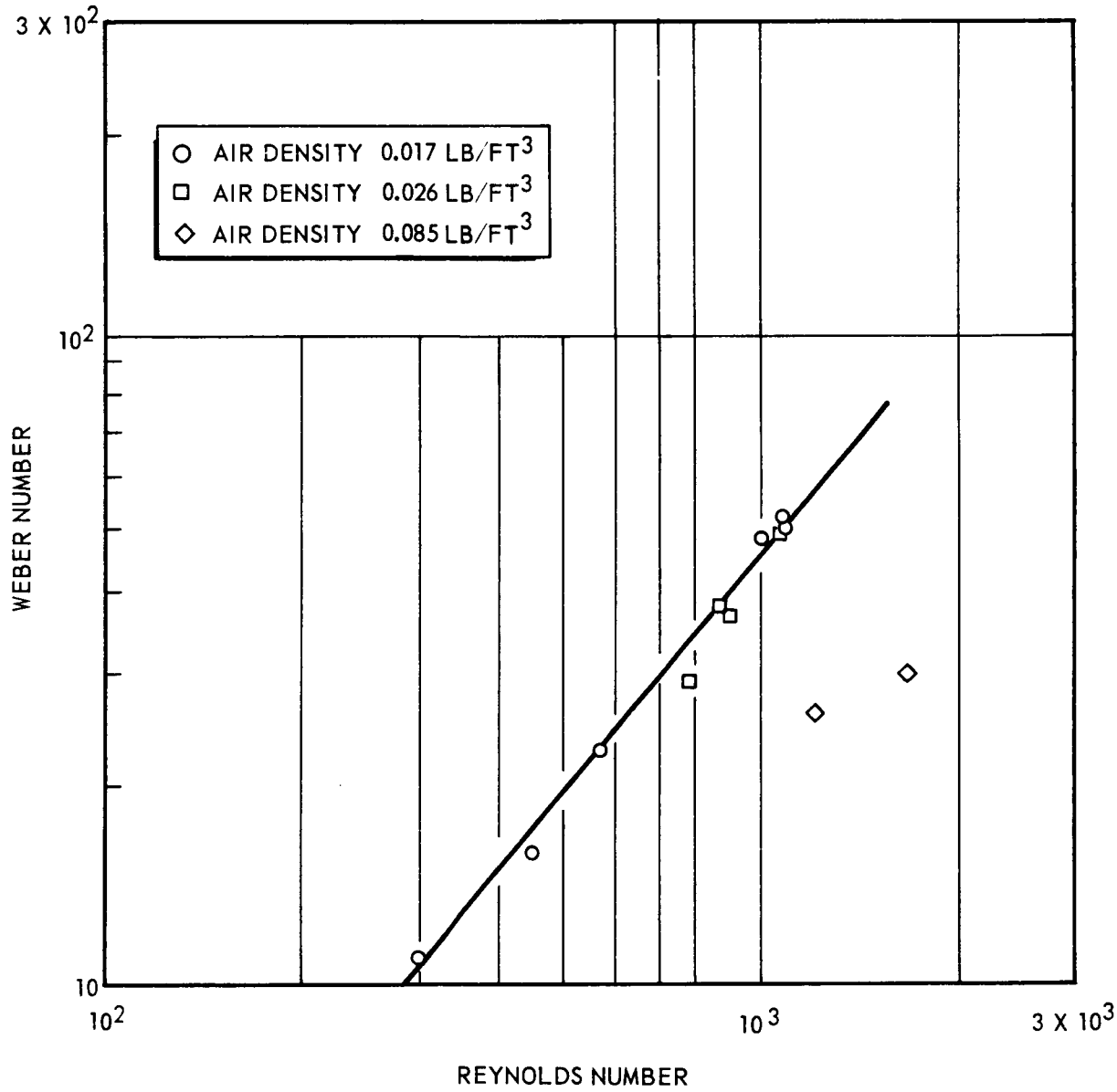

Figure 32. Critical Drop Size Correlation, Water in Air, Data of Ref. 4

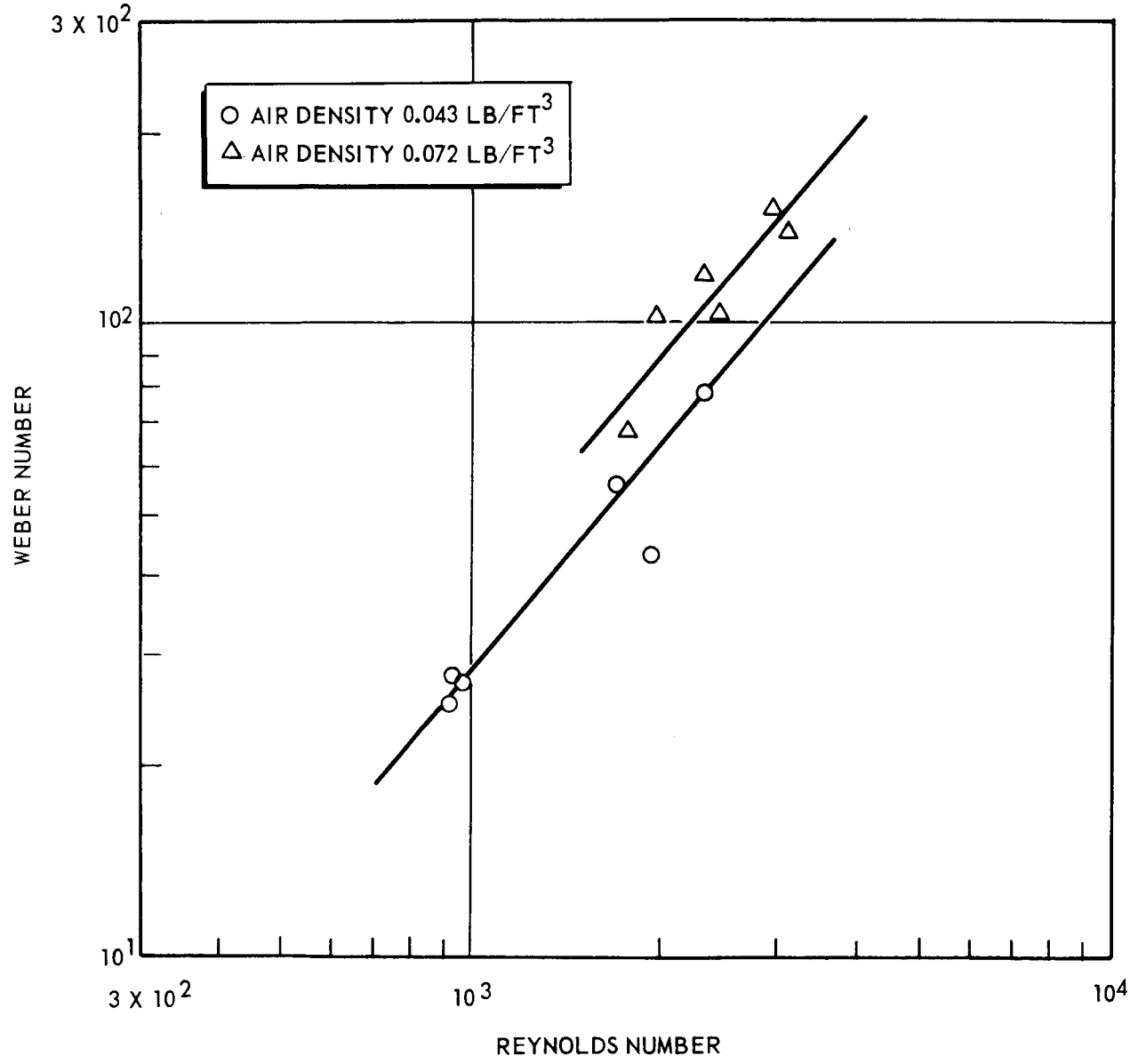

Figure 33. Critical Drop Size Correlation, Glycerin in Air, Data of Ref. 4

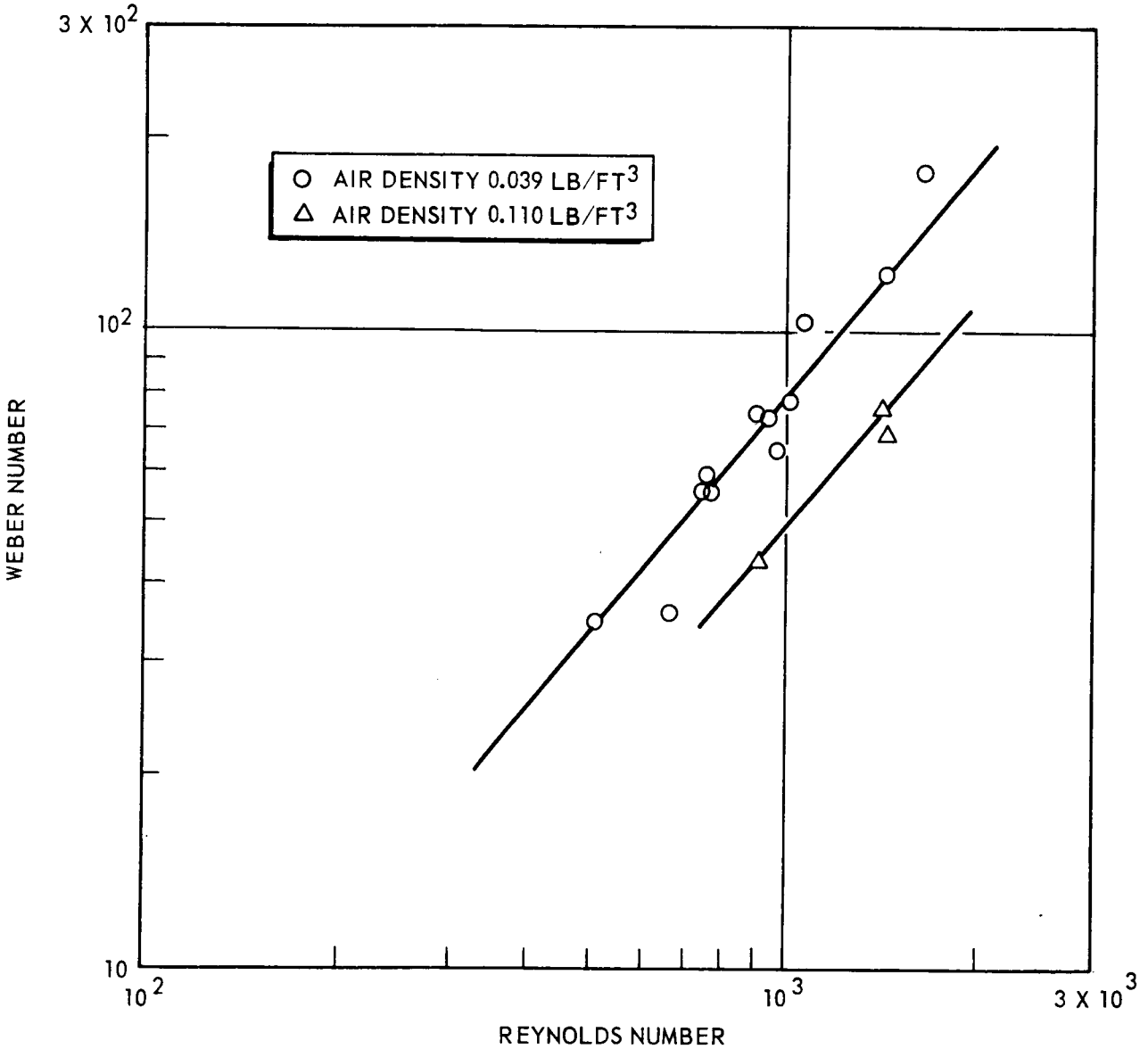

Figure 34. Critical Drop Size Correlation, Methanol in Air, Data of Ref. 4

It is of interest to compare the data of Ref. 7 and 13 (Fig. 31 and 32) In general, the agreement is good and seems to indicate that a functional relationship between Weber and Reynolds number which is more complex than indicated in the previous discussion is needed. The simple relation based on friction coefficient alone seems not to suffice; a much higher power of the Reynolds number (1.2 instead of 0.2) is indicated.

Both of the previous papers dealt with droplets in shear-type breakup. In Ref. 6, bag type breakup is analyzed and the following relation

$$WeRe = \text{constant}$$

seems to hold true for each test series. Comparison of data pertaining to three types of silicone oil are especially instructive. Properties of the oils are

Type of Oil	Viscosity centistoke	Surface Tension dyne/cm	Density g/cc
Silicone Oil No. 1	10	20.14	0.940
Silicone Oil No. 2	50	20.18	0.960
Silicone Oil No. 3	100	20.92	0.970

Evidently the only significant difference between the oils is the viscosity. Test data show that the critical drop sizes are given by the approximate relation

Silicone Oil No. 1 WeRe = 6900
Silicone Oil No. 2 WeRe = 15000
Silicone Oil No. 3 WeRe = 24000

The constants are approximately related by the one-half power of the viscosity.

APPENDIX B

PHYSICAL PROPERTIES OF WATER AND POTASSIUM

Unless otherwise indicated, physical properties for water and potassium used are from:

1. Keenan, J. H. and F. G. Keys: Thermodynamic Properties of Steam, John Wiley & Sons, Inc., New York, 1936.
2. Ewing, C. T., et al.: High-Temperature Properties of Potassium, U.S. Naval Research Laboratory, NRL Report 6233, 24 September 1965.
3. Weatherford, N. D., Jr., et al.: Properties of Inorganic Energy—Conversion and Heat Transfer Fluids for Space Applications, WADD Technical Report 61-96, November 1961.

As indicated in Fig. 35, four different curves for potassium surface tension exists. The values used are indicated on the figure.

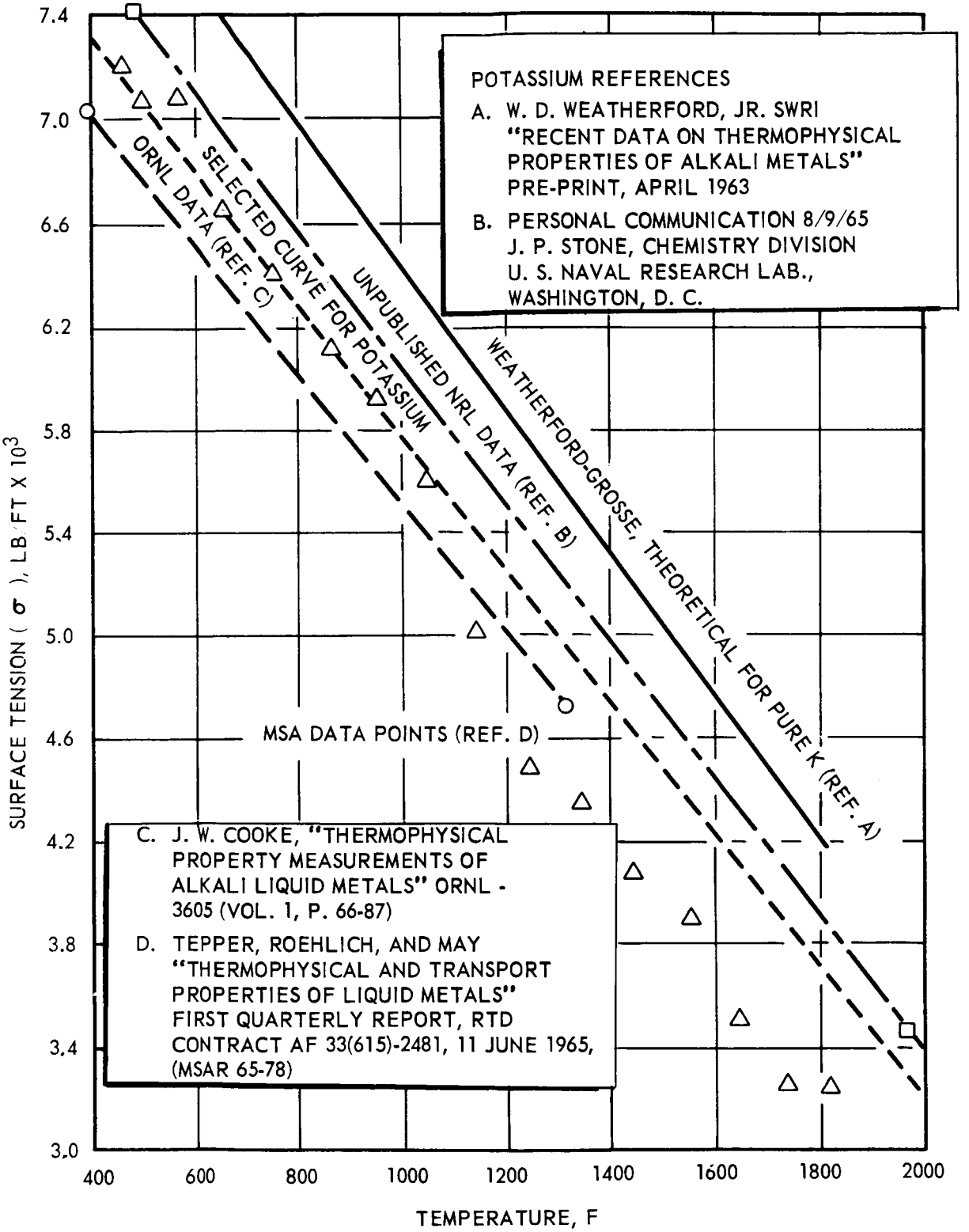

Figure 35. Surface Tension of Liquid Potassium

APPENDIX C

MATERIAL COMPOSITION

Laboratory reports of material composition were received and are shown on the following pages.

ARCEE FOUNDRY, INC.

13900 SOUTH NORWALK BOULEVARD
NORWALK, CALIFORNIA

TO: Rocketdyne
Canoga Park, California

CHEMICAL REPORT ONLY
· CERTIFIED COPY OF TEST REPORTS ·

HEAT NUMBER	SPECIFICATION	MATERIAL	CONDITION
7-21-6		Pure Alum.	F Cond.

— PHYSICAL —

YIELD STRENGTH				TENSILE STRENGTH			
ACTUAL SIZE	ACTUAL AREA	ACTUAL LD. IN LBS.	LBS. PER SQ. INCH	ACTUAL LD. IN LBS.	LBS. PER SQ. INCH	ELON. IN 2"	ELON. %

— CHEMICAL —

SILICON	COPPER	MAGNESIUM	IRON	MANGANESE	TITANIUM	ZINC	BERYL	ALUMINUM
.002	.003	.001	.003					

PURCHASE ORDER NUMBER	PART NUMBER	NUMBER OF PIECES	SHIPPER NUMBER
R63 DDA 838165	N-01262=7	112 pcs.	11313

This is to certify that analysis and test reports governing material specifications are on file for above parts and will be furnished upon request.

Grade 99.99%

ARCEE FOUNDRY, INC.

DATE ~~Sept. x9/21/66~~
9/12/66

BY: E. MacNew

06

ROCKETDYNE • A DIVISION OF NORTH AMERICAN AVIATION, INC.

ARCEE FOUNDRY, INC.

13900 SOUTH NORWALK BOULEVARD
NORWALK, CALIFORNIA

TO:

Rocketdyne
Canoga Park, California

CHEMICAL REPORT ONLY
· CERTIFIED COPY OF TEST REPORTS ·

HEAT NUMBER	SPECIFICATION	MATERIAL	CONDITION
7-15-6A	RBO 170-008	Tens/ 50 Alum.	T6

— PHYSICAL —

YIELD STRENGTH				TENSILE STRENGTH			
ACTUAL SIZE	ACTUAL AREA	ACTUAL LD. IN LBS.	LBS. PER SQ. INCH	ACTUAL LD. IN LBS.	LBS. PER SQ. INCH	ELON. IN 2"	ELON. %

— CHEMICAL —

SILICON	COPPER	MAGNESIUM	IRON	MANGANESE	TITANIUM	ZINC	BERYL	ALUMINUM
7.95	.05	.49	.18	.01	.13	.02	.17	Rem

PURCHASE ORDER NUMBER	PART NUMBER	NUMBER OF PIECES	SHIPPER NUMBER
R63 DDA 838163	N-01262-3	116 pcs.	11212

This is to certify that analysis and test reports governing material specifications are on file for above parts and will be furnished upon request.

ARCEE FOUNDRY, INC.

DATE 7/29/66

BY: E. MacNew

ROCKETDYNE • A DIVISION OF NORTH AMERICAN AVIATION, INC.

ARCEE FOUNDRY, INC.

TEST REPORT

316
~~347~~ **Stainless Steel**

AMS 5360-B

To: Rocketdyne
Canoga Park, California

Date 7/29/66

P.O. No. R63 DDA 838164

Part No. N-01262-5

P/S No. 11213

No. Pcs. 111 pcs.

We hereby certify that the parts shipped on this order were made from materials having the following analysis:

Heat No. 7/15/6

C	.08
Mn	.76
Si	.53
P	.031
S	.019
Ni	12.72
Cr	17.18
Mo	2.08
Cu	.10
Fe	Bal
Cb & TA	----

Tensile Strength	Yield Strength	Elongation	Reduction of Area

Signed E. MacNew
Ed MacNew
Production Control

APPENDIX D

DETERMINATION OF DROPLET VELOCITY

The location of the eroded area observed on the blades makes it possible to estimate the impact velocity of the droplets. This may then be compared to the velocity measured by observing the motion of individual drops in the high-speed films.

Figure 28 clearly shows the area eroded during the tests. Transposition of the line of demarcation to a drawing of the blade profile helps to define the shadow line, or limiting line of impact. Measurement of the limiting angle shows it to be approximately 35 degrees. From a knowledge of the impact angle, the nozzle angle, and the wheel velocity, a velocity diagram can be constructed and the impact velocity measured. In Fig. 36 this velocity is shown as a function of the impact angle.

From data reported in Ref. 14, damage is caused by the normal component of the impact velocity. This component is also shown in Fig. 36, and is observed to be virtually constant, which correlates well with the very uniform appearance of the eroded surface.

The absolute droplet velocity can also be calculated from the velocity diagram, and this value is also shown in Fig. 36. Measurements of observed 350-micron drops show them to be moving at approximately 50 ft/sec prior to impact at the blade row. The velocity of the small drops has not been measured because of difficulty in identifying individual drops in successive frames of film. However, judging from drag coefficient data, these drops must be moving at greater speed than the larger, 350-micron drops (larger drag coefficient).

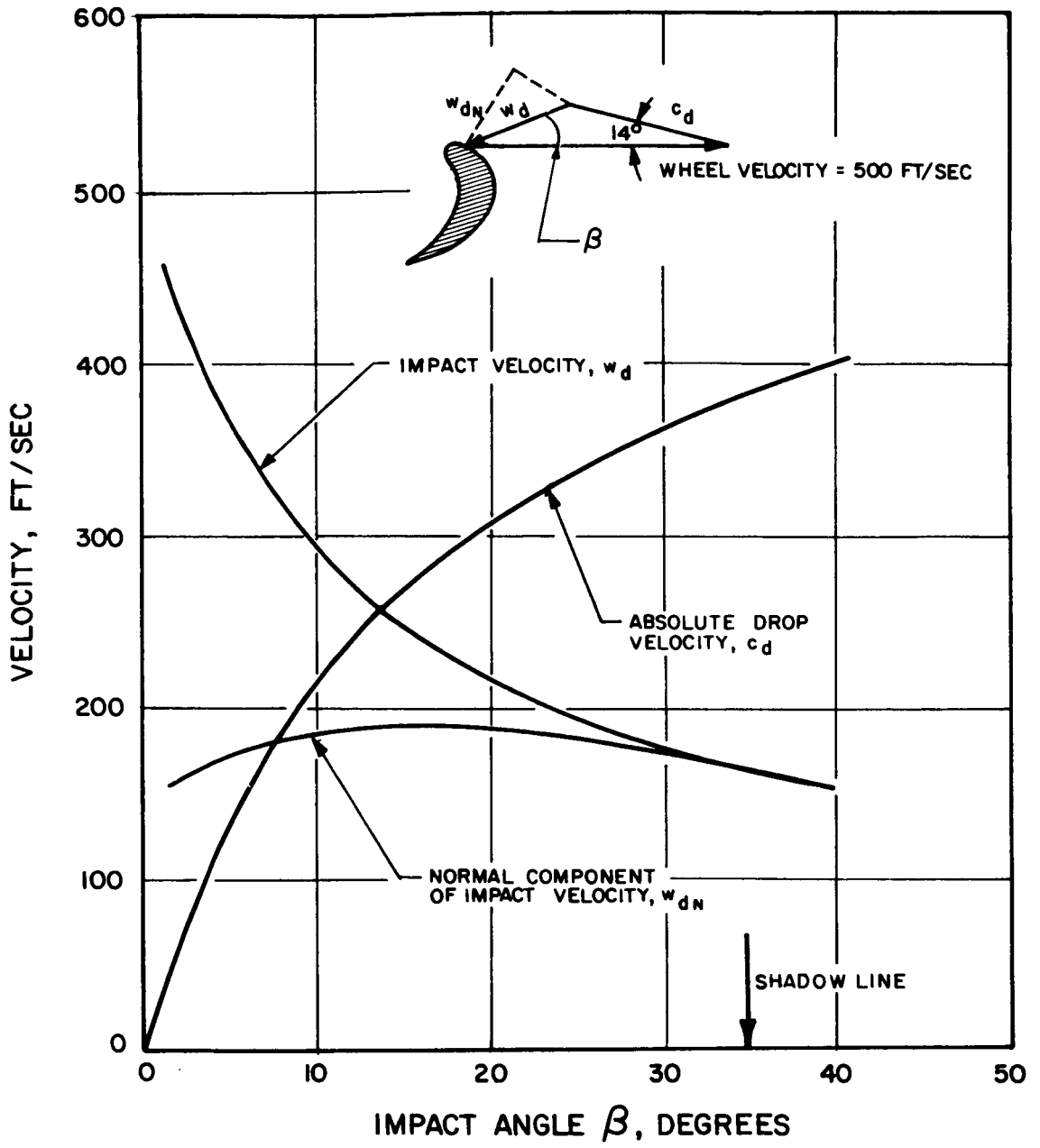

Figure 36. Velocity of Impacting Drops, Tip Velocity 500 ft/sec

UNCLASSIFIED

Security Classification

DOCUMENT CONTROL DATA - R&D

(Security classification of title, body of abstract and indexing annotation must be entered when the overall report is classified)

1. ORIGINATING ACTIVITY *(Corporate author)*
Rocketdyne, a Division of North American Aviation, Inc., 6633 Canoga Avenue, Canoga Park, California

2a. REPORT SECURITY CLASSIFICATION
UNCLASSIFIED

2b. GROUP

3. REPORT TITLE
INVESTIGATION OF VARIABLES IN TURBINE EROSION, DROPLET FORMATION AND MATERIAL DAMAGE WITH STEAM

4. DESCRIPTIVE NOTES *(Type of report and inclusive dates)*
Final Report, 30 June 1965 to 31 October 1966

5. AUTHOR(S) *(Last name, first name, initial)*
Spies, R.

6. REPORT DATE	7a. TOTAL NO. OF PAGES	7b. NO. OF REFS
November 1966	97 & xii	14

8a. CONTRACT OR GRANT NO.	9a. ORIGINATOR'S REPORT NUMBER(S)
NAS7-391	R-6777
b. PROJECT NO.	
c.	9b. OTHER REPORT NO(S) *(Any other numbers that may be assigned this report)*
d.	

10. AVAILABILITY/LIMITATION NOTICES

11. SUPPLEMENTARY NOTES	12. SPONSORING MILITARY ACTIVITY
	NASA, Pasadena

13. ABSTRACT

A program to investigate the effect of variables on turbine erosion is now in progress. Tests have been made with steam to determine the size, velocity, and origin of drops propagating through a typical stage of a space power turbine. Test conditions were chosen to simulate the passage of potassium vapor through the same turbine stage so that correlation with potassium-vapor experiments would be possible in the future. High-speed photographs have been obtained of the vapor flow to evaluate the erosion hazard to turbine blades. To evaluate material characteristics, turbine blades made of four different materials were run in the same wheel. Comparative weight-loss data and rate-of-loss data permit evaluation based on material properties. This evaluation is continuing. Tests with different quality, speed, and nozzle-to-rotor spacing are being conducted. Future reports will be issued on the results of these investigations.

DD FORM 1 JAN 64 1473

UNCLASSIFIED

Security Classification

14. KEY WORDS	LINK A		LINK B		LINK C	
	ROLE	WT	ROLE	WT	ROLE	WT
Turbine Erosion						
Steam						
Materials						
Droplets						

INSTRUCTIONS

1. ORIGINATING ACTIVITY: Enter the name and address of the contractor, subcontractor, grantee, Department of Defense activity or other organization *(corporate author)* issuing the report.

2a. REPORT SECURITY CLASSIFICATION: Enter the overall security classification of the report. Indicate whether "Restricted Data" is included. Marking is to be in accordance with appropriate security regulations.

2b. GROUP: Automatic downgrading is specified in DoD Directive 5200.10 and Armed Forces Industrial Manual. Enter the group number. Also, when applicable, show that optional markings have been used for Group 3 and Group 4 as authorized.

3. REPORT TITLE: Enter the complete report title in all capital letters. Titles in all cases should be unclassified. If a meaningful title cannot be selected without classification, show title classification in all capitals in parenthesis immediately following the title.

4. DESCRIPTIVE NOTES: If appropriate, enter the type of report, e.g., interim, progress, summary, annual, or final. Give the inclusive dates when a specific reporting period is covered.

5. AUTHOR(S): Enter the name(s) of author(s) as shown on or in the report. Enter last name, first name, middle initial. If military, show rank and branch of service. The name of the principal author is an absolute minimum requirement.

6. REPORT DATE: Enter the date of the report as day, month, year; or month, year. If more than one date appears on the report, use date of publication.

7a. TOTAL NUMBER OF PAGES: The total page count should follow normal pagination procedures, i.e., enter the number of pages containing information.

7b. NUMBER OF REFERENCES: Enter the total number of references cited in the report.

8a. CONTRACT OR GRANT NUMBER: If appropriate, enter the applicable number of the contract or grant under which the report was written.

8b, 8c, & 8d. PROJECT NUMBER: Enter the appropriate military department identification, such as project number, subproject number, system numbers, task number, etc.

9a. ORIGINATOR'S REPORT NUMBER(S): Enter the official report number by which the document will be identified and controlled by the originating activity. This number must be unique to this report.

9b. OTHER REPORT NUMBER(S): If the report has been assigned any other report numbers *(either by the originator or by the sponsor)*, also enter this number(s).

10. AVAILABILITY/LIMITATION NOTICES: Enter any limitations on further dissemination of the report, other than those imposed by security classification, using standard statements such as:

(1) "Qualified requesters may obtain copies of this report from DDC."

(2) "Foreign announcement and dissemination of this report by DDC is not authorized."

(3) "U. S. Government agencies may obtain copies of this report directly from DDC. Other qualified DDC users shall request through _____."

(4) "U. S. military agencies may obtain copies of this report directly from DDC. Other qualified users shall request through _____."

(5) "All distribution of this report is controlled. Qualified DDC users shall request through _____."

If the report has been furnished to the Office of Technical Services, Department of Commerce, for sale to the public, indicate this fact and enter the price, if known.

11. SUPPLEMENTARY NOTES: Use for additional explanatory notes.

12. SPONSORING MILITARY ACTIVITY: Enter the name of the departmental project office or laboratory sponsoring *(paying for)* the research and development. Include address.

13. ABSTRACT: Enter an abstract giving a brief and factual summary of the document indicative of the report, even though it may also appear elsewhere in the body of the technical report. If additional space is required, a continuation sheet shall be attached.

It is highly desirable that the abstract of classified reports be unclassified. Each paragraph of the abstract shall end with an indication of the military security classification of the information in the paragraph, represented as *(TS)*, *(S)*, *(C)*, or *(U)*.

There is no limitation on the length of the abstract. However, the suggested length is from 150 to 225 words.

14. KEY WORDS: Key words are technically meaningful terms or short phrases that characterize a report and may be used as index entries for cataloging the report. Key words must be selected so that no security classification is required. Identifiers, such as equipment model designation, trade name, military project code name, geographic location, may be used as key words but will be followed by an indication of technical context. The assignment of links, rules, and weights is optional.